doi:10.1093/plcell/koab123

THE PLANT CELL

THE PLANT CELL 2021: 33: 2479–2505

Research Article

Loss of inner-envelope K^+/H^+ exchangers impairs plastid rRNA maturation and gene expression

Rachael Ann DeTar [1], Rouhollah Barahimipour [2], Nikolay Manavski [3], Serena Schwenkert [3], Ricarda Höhner,[1] Bettina Bölter,[3] Takehito Inaba [4], Jörg Meurer [3], Reimo Zoschke [2] and Hans-Henning Kunz [1,3,*,†]

1 Plant Physiology, School of Biological Sciences, Washington State University, PO Box 644236, Pullman, WA 99164-4236, USA
2 Max Planck Institute of Molecular Plant Physiology, Wissenschaftspark Golm, Am Mühlenberg 1, 14476 Potsdam, Germany
3 Plant Sciences, Department I, LMU Munich, Großhaderner Str. 2-4, 82152 Planegg-Martinsried, Germany
4 Department of Agricultural and Environmental Sciences, Faculty of Agriculture, University of Miyazaki, Miyazaki 889-2192, Japan

*Author for correspondence: kunz@lmu.de
†Senior author

H.-H.K. designed research. R.A.D. performed most of the experiments with further support from S.S. and B.B. R.B. and R.Z. performed plastome microarray and RNA blot experiments and analyzed the data. N.M. and J.M. carried out structural RNA probing, RNA-Co-IP, and polysome analysis. R.H. analyzed elemental composition of leaf tissue. T.I. quantified GLK1 protein level in mutants. B.B. carried out protein import studies. H.-H.K. and R.A.D. wrote the paper together with edits from B.B., S.S., R.B., N.M., T.I., J.M., and R.Z. H.-H.K. are responsible for contact and ensuring communication.
The author responsible for distribution of materials integral to the findings presented in this article in accordance with the policy described in the Instructions for Authors (https://academic.oup.com/plcell) is: Hans-Henning Kunz, kunz@lmu.de

Abstract

The inner-envelope K^+ EFFLUX ANTIPORTERS (KEA) 1 and 2 are critical for chloroplast development, ion homeostasis, and photosynthesis. However, the mechanisms by which changes in ion flux across the envelope affect organelle biogenesis remained elusive. Chloroplast development requires intricate coordination between the nuclear genome and the plastome. Many mutants compromised in plastid gene expression (PGE) display a virescent phenotype, that is delayed greening. The phenotypic appearance of *Arabidopsis thaliana kea1 kea2* double mutants fulfills this criterion, yet a link to PGE has not been explored. Here, we show that a simultaneous loss of KEA1 and KEA2 results in maturation defects of the plastid ribosomal RNAs. This may be caused by secondary structure changes of rRNA transcripts and concomitant reduced binding of RNA-processing proteins, which we documented in the presence of skewed ion homeostasis in *kea1 kea2*. Consequently, protein synthesis and steady-state levels of plastome-encoded proteins remain low in mutants. Disturbance in PGE and other signs of plastid malfunction activate GENOMES UNCOUPLED 1-dependent retrograde signaling in *kea1 kea2*, resulting in a dramatic downregulation of GOLDEN2-LIKE transcription factors to halt expression of photosynthesis-associated nuclear-encoded genes (PhANGs). PhANG suppression delays the development of fully photosynthesizing *kea1 kea2* chloroplasts, probably to avoid progressing photo-oxidative damage. Overall, our results reveal that KEA1/KEA2 function impacts plastid development via effects on RNA-metabolism and PGE.

Introduction

Biochemical pathways in eukaryotic cells are compartmentalized in different membrane-bound organelles with characteristic ion and pH compositions maintained by transport proteins. The maintenance of ion and proton gradients across cell membranes and within subcellular compartments is termed 'homeostasis' (Chanroj et al., 2012; Höhner et al., 2016a).

Received February 19, 2021. Accepted April 30, 2021. Advance access publication May 7, 2021

IN A NUTSHELL

Background: Proteins that transport simple charged molecules (ions) are components of all plant cell membranes, including chloroplast membranes. Chloroplast envelope membranes delineate the chloroplast from the rest of the cell, and the thylakoid membranes house many proteins used for photosynthesis. Each of these membranes contains its own set of ion transport proteins. The space between the envelope and thylakoid membranes is called the stroma. Ion transporters are responsible for maintaining the balance of ions or "ion homeostasis" of the stroma. The stroma contains a small genome with ~120 genes left over from the chloroplasts' bacterial ancestor, as well as ribosomes and other machinery needed for gene expression. The expression of the chloroplast genome in coordination with genes in the nucleus is essential for chloroplast development and function. However, little is known about how ion homeostasis influences the expression of the chloroplast genome.

Question: We wanted to know if disrupting ion homeostasis would influence plastid gene expression, and in turn impair chloroplast development. This was inspired by the observation that losing two genes for K^+ ion transporters in the chloroplast envelope, *KEA1* and *KEA2*, delayed leaf greening and caused underdeveloped chloroplasts in *Arabidopsis thaliana* plants.

Findings: Plants missing KEA1 and KEA2 struggled to complete RNA maturation—the process where a newly transcribed RNA is cut or otherwise altered—in the chloroplast. Our experiments showed that the nuclear-encoded helper proteins for RNA maturation struggled to bind their stromal partner RNA in plants missing KEA1 and KEA2. This defect was prominent for chloroplast ribosomal RNAs. Correspondingly, there were fewer functional ribosomes, and chloroplast protein synthesis rates were low in mutants. As a result, plants missing KEA1 and KEA2 lack enough important chloroplast proteins, and thus remain underdeveloped.

Next steps: We have an intriguing hypothesis that KEA1 and KEA2 activity is altered to regulate chloroplast gene expression, and hence chloroplast development. We want to investigate this hypothesis by testing if these transporter proteins interact directly with components of the chloroplast gene expression machinery, and if doing so influences ion transport activity. Our research has revealed a role for ion transporters in the plant cell.

Of particular importance for ion and pH homeostasis are $K^+(Na^+)/H^+$ exchangers, which are highly abundant in plant cells (Pittman, 2012; Sze and Chanroj, 2018). These carriers link internal ion and proton levels. Bioenergetic organelles such as the chloroplast and mitochondrion build up steep pH and ion gradients across membranes, and thus invest considerable energy in ion homeostasis. Both compartments harness the gradients' potential energy, collectively known as proton-motive force (PMF), to supply the cell with ATP and other high energy compounds. Chloroplasts use photosynthesis to convert solar energy into PMF and then into chemical bonds. This process provides carbon and chemical energy for most organisms on earth. Thus, the chloroplast is a highly relevant target of ion homeostasis research. In recent years, there has been substantial progress in identifying transporters and channels that maintain subcellular ion gradients within the plastid (Finazzi et al., 2015; Szabò and Spetea, 2017).

In this study, we focus on the physiological role of two members from the K^+-efflux antiporter family, KEA1 and KEA2, which facilitate K^+/H^+ exchange across the chloroplast inner envelope membrane in *Arabidopsis thaliana* (Aranda-Sicilia et al., 2012; Aranda Sicilia et al., 2021). A simultaneous loss of both carriers results in stunted mutant plants with elevated leaf K^+ content (Kunz et al., 2014; Höhner et al., 2019). The photosynthetic efficiency is dramatically reduced in *kea1 kea2* even though the stromal pH in illuminated mutant chloroplasts is only mildly affected (Kunz et al., 2014; Aranda Sicilia et al., 2021). Since the volume of *kea1 kea2* leaf plastids is increased, it is expected that in wild-type (WT) plants KEA1/KEA2 facilitates K^+ efflux from the stroma to adjust the osmotic potential of the organelle. KEA1 and KEA2 are also relevant for chloroplast biogenesis, as the double mutants display pale young leaves with immature chloroplasts (Aranda-Sicilia et al., 2016). However, the mechanistic role of envelope ion transport via KEA1/KEA2 in plastid development remains an outstanding scientific question (Sze and Chanroj, 2018). Therefore, the rationale of this research was to understand the connection between these two processes and their relationship to photosynthesis.

Chloroplasts develop during the plant life cycle from photosynthetically inactive proplastids in the meristems through coordinated expression of specific genes (Pogson and Albrecht, 2011; Hernandez-Verdeja and Strand, 2018). This coordination is complex because plastids have retained a small genome of approximately 120 genes known as the plastome, which is essential for chloroplast function (de Vries and Archibald, 2018). The plastome encodes several components of the electron transport chain, including the photosystem reaction centers (Allen et al., 2011). During endosymbiosis, the majority of chloroplast genes were transferred to the nuclear genome. Many conserved and newly evolved nuclear genes encoding chloroplast proteins, including chlorophyll biosynthesis enzymes and the light-harvesting machinery, are collectively known as the photosynthesis-associated nuclear-encoded genes (PhANGs) (Berry et al., 2013).

Notably, many photosynthetic protein complexes including the photosystems, the cytochrome b_6f complex, ATP synthase, and ribulose-1,5-bisphosphate-carboxylase (RuBisCo) contain subunits from both genomes (Allen et al., 2011). The division of genes encoding the chloroplast proteome between the nuclear and plastid genomes necessitates tight regulation and communication between the two genetic compartments to balance protein stoichiometry (Woodson and Chory, 2008). Nucleus to plastid communication to moderate plastid gene expression (PGE) is known as anterograde signaling. Anterograde signaling impacts PGE at the transcriptional, posttranscription, and translational level via nuclear-encoded plastid RNA polymerases (NEPs), prokaryotic-type RNA polymerase-associated proteins (PAPs), and chloroplast RNA-binding proteins (cRBPs) that are posttranslationally imported into plastids (Barkan and Small, 2014; Zoschke and Bock, 2018). cRBPs assist in stabilizing, end processing, splicing, and editing of mRNAs and rRNAs (Schmitz-Linneweber and Small, 2008; Hammani et al., 2014). Intriguingly, many mutants defective in anterograde control of PGE display a distinctive 'virescent' (delayed greening) phenotype (Zhou et al., 2009). In virescent mutants, young leaves remain pale and contain underdeveloped poorly photosynthesizing chloroplasts, whereas older leaves recover to a certain extent levels of chlorophyll and photosynthetic proteins.

Communication from the chloroplast to nucleus to moderate nuclear gene expression is referred to as retrograde signaling (RS) (Kleine and Leister, 2016). The RS pathway is activated in response to various plant stressors, chloroplast damage, and by changes in PGE (Leister et al., 2017). While the exact nature of the signal(s) sent back to the nucleus remains poorly understood, RS has been shown to alter nuclear gene expression and prevent oxidative damage (Cheng et al., 2011; Woodson, 2016; D'Alessandro et al., 2018; Kacprzak et al., 2019). Little is known about a potential role of RS in response to perturbation of the plastid ion homeostasis. This is somewhat surprising, as many stages of PGE including RNA folding, RNA–protein interactions, and ribosomal activity rely on the prevalent ion and pH conditions (Bhaya and Jagendorf, 1984; Horlitz and Klaff, 2000; Draper et al., 2005; McDermott et al., 2018; Gawroński et al., 2020). These buffer conditions are disrupted when abiotic stress or alteration of ion transport offsets plastid ion homeostasis (Schroppelmeier and Kaiser, 1988). Although it remains unclear how the stromal ion–pH–RNA interplay is orchestrated, we hypothesized that plastid $K^+(Na^+)/H^+$ exchangers such as those from the KEA family might be involved.

While the pale young leaf phenotype in *kea1 kea2* double mutants has been noted before (Aranda-Sicilia et al., 2016), it has not been investigated if it constitutes a virescent phenotype resulting from changes in PGE. Intriguingly, the pale young leaf phenotype in *kea1 kea2* mutants can be suppressed by exposing plants to salt stress (Kunz et al., 2014). This behavior suggests that *kea1 kea2* may serve as a useful model to gain insights into the relationship between chloroplast ion homeostasis and PGE. Furthermore, investigation of PGE may also provide a mechanistic explanation for the delayed chloroplast biogenesis documented in *kea1 kea2* loss-of-function lines and thus answer one of the outstanding questions in the field (Sze and Chanroj, 2018). Using transcriptomics combined with the salt recovery phenomenon in *kea1 kea2*, we set out to gain insights into the molecular basis of the *kea1 kea2* phenotype and its potential connection to PGE.

Results

Insights into the molecular consequences of disturbed chloroplast ion transport using nuclear transcriptomics

The loss of KEA1/KEA2 function in the two previously isolated independent T-DNA double-mutant insertion lines (*kea1-1 kea2-1* and *kea1-2 kea2-2* [Kunz et al., 2014]) resulted in decreased maximum quantum yield of photosystem II (PSII) (Figure 1, A and B; F_v/F_m). In addition, both double mutants exhibited lower steady-state PSII quantum yield (Figure 1C; ΦII), and higher quantum yield of regulated nonphotochemical energy loss in PSII (Figure 1D; ΦNPQ) compared with WT plants (Col-0). The quantum yield of nonregulated nonphotochemical energy loss in PSII (Figure 1E; ΦNO) remained unchanged. Interestingly, PSII-related parameters in both *kea1 kea2* lines recovered drastically under moderate salt stress as shown by a significant increase in F_v/F_m (Figure 1B; Kunz et al., 2014)). The NaCl-treated *kea1 kea2* plants were also homogenously greener compared with control conditions. Whereas WT individuals grew smaller under NaCl stress, mutant plants did not exhibit a similar size reduction after treatment. The rescue effect was specific for NaCl. Treatments with equimolar KCl did not recover *kea1 kea2* plants but worsened the mutants' performance (Supplemental Figure S1). Next up, we determined the leaf ionome of WT and mutant plants grown in the presence or absence of exogenous NaCl (Table 1). In line with previous studies (Höhner et al., 2016b, 2019), *kea1 kea2* lines exhibited elevated potassium (K) and phosphorus (P) but decreased magnesium (Mg) levels. When exposed to salt stress, sodium (Na) accumulated in all genotypes to a similar degree. The levels of K, Mg, and all other elements in both *kea1 kea2* lines were also equivalent to the WT under these conditions. Due to the specific recovery effect of NaCl on photosynthesis and the leaf ionome of *kea1kea2*, we employed the salt treatment rescue to dissect the molecular consequences of decreased K^+/H^+ exchange across the plastid envelope membrane.

Aerial tissue from WT plants and the two independent T-DNA double-mutant *kea1 kea2* lines grown on control and NaCl media as shown in Figure 1A were harvested. Subsequently, total mRNA was extracted, converted into a cDNA library, and sequenced on an Illumina platform. The standard Tuxedo Suite software was used for transcript alignment and differential expression analysis (Trapnell et al., 2012).

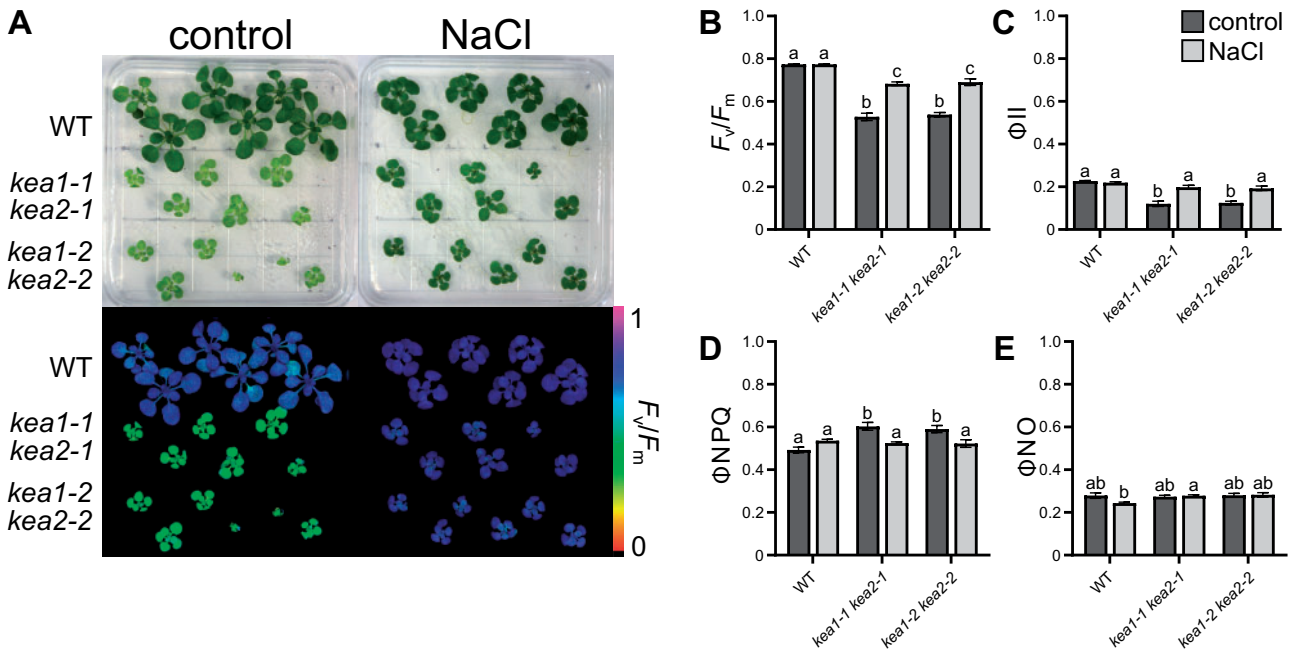

Figure 1 NaCl treatment rescues the *kea1 kea2* photosynthetic phenotype. A WT and two independent *kea1 kea2* T-DNA loss-of-function lines grown on ½ MS control or with NaCl treatment. Control treatment was to simply grow plants on ½ MS media until harvest, transferring to fresh regular ½ MS media one week after germination. NaCl treatment was to grow plants on ½ MS media supplemented with 67.5 mM NaCl for 2 weeks beginning 1 week after germination on regular ½ MS media. Lower panels display false color image of maximum quantum yield of PSII (F_v/F_m). B–E, Bar graph of mean chlorophyll fluorescence parameter in WT and *kea1 kea2* under control (dark gray bars) or NaCl treatment (light gray bars) (±SEM, $n = 6$). Parameters include (B) F_v/F_m, (C) quantum yield of PSII abv. ΦII, (D) quantum yield of regulated non-photochemical quenching abv. ΦNPQ, and (E) non-regulated non-photochemical quenching, abv. ΦNO. Different letters denote significantly different means based on an ordinary two-way ANOVA with Tukey's multiple comparisons test ($P < 0.05$).

Table 1 Leaf-level concentrations of elements (μg*mg DW $^{-1}$)

	WT				*kea1-1kea2-1*				*kea1-2 kea2-2*			
	Control		NaCl		Control		NaCl		Control		NaCl	
Element	Mean	Std. Err.	Mean	Std. Err.	Mean	Std. Err.	Mean	Std. Err.	Mean	Std. Err.	Mean	Std. Err.
Na	0.54	0.11	14.56	2.23	1.23	0.33	15.89	3.07	1.30	0.45	17.74	1.84
Mg	5.78	0.76	5.34	0.20	**3.10**	**0.34**	5.31	0.18	**3.69**	**0.24**	4.77	0.62
P	8.10	0.53	7.13	0.35	**11.54**	**0.69**	**11.11**	**2.10**	**11.96**	**0.40**	7.82	0.21
S	4.37	0.58	7.06	0.32	5.15	0.31	8.20	0.87	6.30	0.90	6.64	0.32
Cl	1.22	0.08	11.72	1.40	1.15	0.11	10.66	0.89	1.40	0.29	11.89	1.28
K	40.59	2.15	29.37	1.39	**51.68**	**0.99**	31.91	1.95	**53.11**	**1.80**	29.88	0.76
Ca	36.07	3.09	32.27	1.52	41.83	8.72	28.85	1.61	34.36	4.29	34.61	6.12
Mn	0.08	0.00	0.08	0.00	**0.12**	**0.02**	0.09	0.01	0.10	0.01	0.11	0.01
Fe	0.14	0.02	0.12	0.01	0.22	0.05	0.09	0.01	0.18	0.05	0.15	0.03
Cu	0.01	0.00	0.01	0.00	0.02	0.00	0.01	0.00	0.06	0.04	0.01	0.00
Zn	0.73	0.13	0.50	0.10	1.02	0.29	0.51	0.07	1.05	0.45	0.39	0.07
Rb	0.01	0.00	0.01	0.00	0.01	0.00	0.01	0.00	0.01	0.00	0.01	0.00
Sr	0.06	0.01	0.05	0.00	0.07	0.01	0.05	0.01	0.06	0.01	0.08	0.02
Pb	0.15	0.04	0.11	0.03	0.18	0.03	0.06	0.02	0.16	0.04	0.09	0.02

Mean leaf concentration of assorted elements normalized to dry weight (μg*mg DW $^{-1}$) and standard error of the mean (Std. Err., $n = 6$–7). Bolded values indicate statistically significantly different means from correspondingly treated WT sample based on Dunnett's or Dunn's multiple comparison test ($P < 0.05$).

Each sample had high coverage and sequence quality (Supplemental Table S1). Furthermore, principal component analysis of gene expression values output from Cufflinks indicated that most variance in gene expression results from sample identity, as sample replicates cluster tightly in relation to the first principal component, which accounted for 69.5% of the variance (PC1, Supplemental Figure S2).

Under control conditions, 3630 differentially expressed genes (DEGs) were identified when comparing WT and both *kea1 kea2* double-mutant lines (Supplemental Table S2 and Supplemental Figure S3). Interestingly, when WT and *kea1*

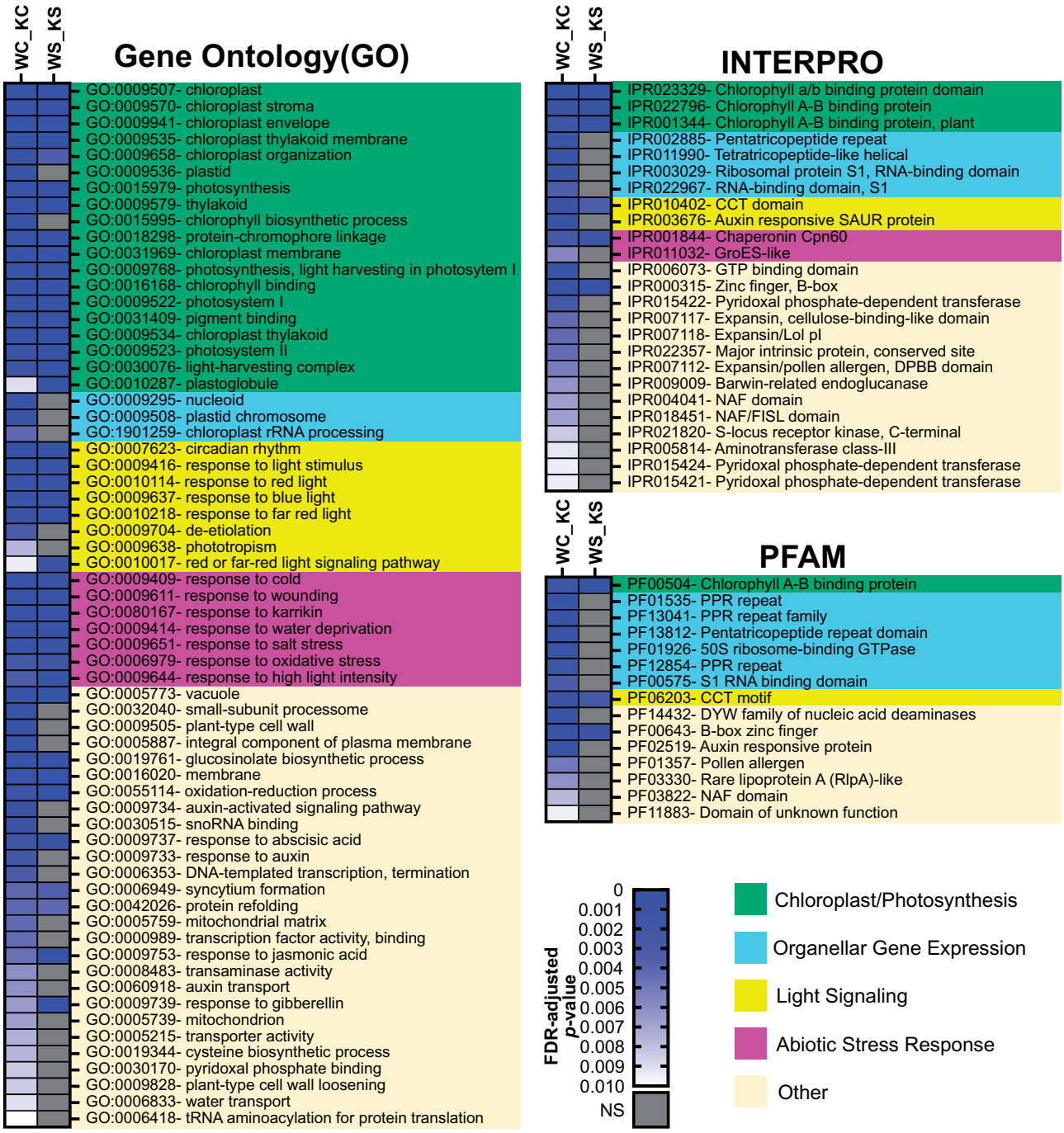

Figure 2 Functional enrichment analysis reveals that significantly DEGs in *kea1 kea2* compared with the WT under control conditions are often associated with specific GO terms, INTERPRO domains and PFAM families. Some terms, domains, and families are no longer significantly enriched when comparing *kea1 kea2* and WT when both are treated with NaCl. FUNC-E functional enrichment analysis of DEG lists comparing the consensus of both *kea1 kea2* lines to WT under control (left column; WC_KC) and NaCl treatment (right column; WS_KS). Control and NaCl treatments are as described for Figure 1. The most significantly enriched annotations from the WC_KC comparison (FDR-adjusted $P < 0.01$) are shown with corresponding results for the WS_KS comparison. GO terms, INTERPRO domains and PFAM families were used as the ontologies for analysis. Color scale of boxes corresponding to each term represent smaller P values (i.e. more significant = deeper blue). Gray boxes denote nonsignificantly enriched annotations (FDR-adjusted $P \geq 0.01$). Color blocks over text correspond to a broad functional description of those annotations.

kea2 were compared under salt stress conditions, which rescue development and photosynthesis in double mutants, the number of DEGs decreased to only 1,109 genes (Supplemental Table S2 and Supplemental Figure 3). According to the Arabidopsis protein subcellular localization database SUBA4 (Hooper et al., 2017), there was an approximately two-fold over-representation of *A. thaliana* genes encoding chloroplast-localized proteins in the DEG list for

the control-treated WT versus *kea1 kea2* compared with the High Confidence Marker standard (Supplemental Figure S4, A and B). For the DEG list comparing NaCl-treated WT with NaCl-treated *kea1 kea2* (Supplemental Figure S4C), there was a three-fold overrepresentation of chloroplast-targeted genes compared with the high-confidence-marker (HCM) standard (Supplemental Figure S4A). Thus, *kea1 kea2* disproportionately alters the expression of chloroplast-targeted gene products under both treatments. The two lists of DEGs only shared 242 upregulated genes, and 358 downregulated genes, suggesting that many of the genes that are deregulated in mutant plants under control conditions are no longer differentially expressed compared with WT after salt treatment (Supplemental Figure S5).

Functional enrichment analyses provide evidence that PGE is affected by loss of KEA1/KEA2

To deduce functional information from the nuclear transcriptomic dataset, we employed the functional enrichment tool FUNC-E (Ficklin and Alex Feltus, 2018). We drew on information from three independent annotation systems to do our analysis: molecular function, cellular component, and biological process terms from the Gene Ontology (GO) database, protein domains from InterPro, and protein families from PFAM. Briefly, the more DEGs assigned to a particular annotation (i.e. GO term, PFAM family, InterPro domain), the lower the false discovery rate (FDR)-adjusted *P* value for this annotation (Figure 2). We use the word "annotation" to refer to a specific term, family, domain, or class from the aforementioned databases.

Supporting our previous finding that genes encoding chloroplast-targeted proteins were overrepresented in our dataset (Supplemental Figure S4), we found most enriched GO terms when comparing WT to *kea1 kea2* under control conditions (WC_KC) related to the broad categories of chloroplast/photosynthesis, light signaling, and abiotic stress response (Figure 2). Protein domains and families relating to all three of these categories were also enriched based on InterPro and PFAM databases, corroborating the notion that loss of the inner envelope carriers KEA1 and KEA2 primarily impacts key processes linked to chloroplast function. Furthermore, we found enrichment in six GO terms assigned to abiotic stress factors, namely cold, wounding, drought, salt, and oxidative stress. Many of these annotations were also significantly enriched under salt, so were unlikely to be causal for the *kea1 kea2* phenotype.

To gain insight into the delayed greening phenotype in *kea1 kea2* mutants, we focused on annotations that were significantly enriched in the WC_KC comparison, but not in the NaCl-treated WT-*kea1 kea2* comparison (WS_KS). This approach unveiled several GO terms, which prompted further investigations. First, enrichment of the term "chlorophyll biosynthesis" (GO:0015995) supported earlier results showing reduced chlorophyll levels in *kea1 kea2* and subsequent NaCl-mediated recovery (Kunz et al., 2014). Additionally, several GO terms related to organellar gene expression triggered our interest, as PGE is a key process required for chloroplast development (Bollenbach et al., 2005; Stoppel and Meurer, 2011; Tiller and Bock, 2014). PGE-related terms included "nucleoid" (GO:0009295), "plastid chromosome" (GO:0009508), and "chloroplast rRNA processing" (GO:1901259). Furthermore, analysis with InterPro and PFAM databases revealed that nuclear-encoded proteins related to organellar gene expression were enriched under the control treatment, but not under salt treatment. These included organellar RNA-binding proteins such as pentatricopeptide repeat (PPR) proteins (IPR002885, PF13812) and ribosome-binding proteins (IPR003029, PF01926). This trend suggests the delayed leaf greening and chloroplast development in *kea1 kea2* may be related to alterations in chloroplast RNA processing, ribosome assembly, and/or general PGE.

A closer look at the individual genes with respective annotations of interest (Figure 3; Supplemental Dataset 5) showed that transcripts were not uniformly deregulated in one direction. For instance, in the case of the annotation "chloroplast organization" (GO:0009658; Figure 3A), we found that only about 20% of the transcripts were suppressed, and the remaining transcripts increased in expression in the WC_KC comparison. Interestingly, two of the most suppressed genes with this annotation encode the GOLDEN2-LIKE1 (*GLK1*) and GOLDEN2-LIKE2 (*GLK2*) transcription factors (TFs). Together, GLK1/GLK2 coordinate the expression of many PhANGs and genes controlling chloroplast development (Waters et al., 2008, 2009). Both TF mRNAs return to WT levels under salt recovery. In the case of "chlorophyll biosynthesis" (GO:0015995; Figure 3B), about 50% of DEGs were suppressed, but the other half increased in expression. Notably, many downregulated genes associated with this GO term encode proteins, which catalyze or regulate committed steps in the chlorophyll biosynthesis pathway during de-etiolation. These include HEMA1 (McCormac et al., 2001), GUN4 (Adhikari et al., 2011), PORA (Paddock et al., 2012), and DXS (Mandel et al., 1996; Estévez et al., 2001). The transcripts that increased in expression were generally not involved in key chlorophyll biosynthesis reactions. Gene transcripts, annotated with "de-etiolation" (GO:0009704; Figure 3C), were also primarily downregulated. In contrast, transcripts associated with organellar gene expression-related annotations (Ribosomal protein S1, IPR003029; "Plastid Chromosome", GO:009508; PPR Domain, PF13812; 50S Ribosome Binding GTPase, PF01926; and "Plastid rRNA Processing", GO:1901259) were almost universally significantly upregulated in *kea1kea2*, although the degree of transcript increase varied (Figure 3, D–H). Across all annotations, we observed a reversion of most of these effects on gene expression in salt-stressed plants, i.e. the transcription of two independent *kea1 kea2* mutants behaved more similarly to WT under salt stress conditions.

Additionally, even some annotations still significantly enriched under salt treatment in the FUNC-E analysis displayed partial salt-mediated recovery of specific gene expression. These

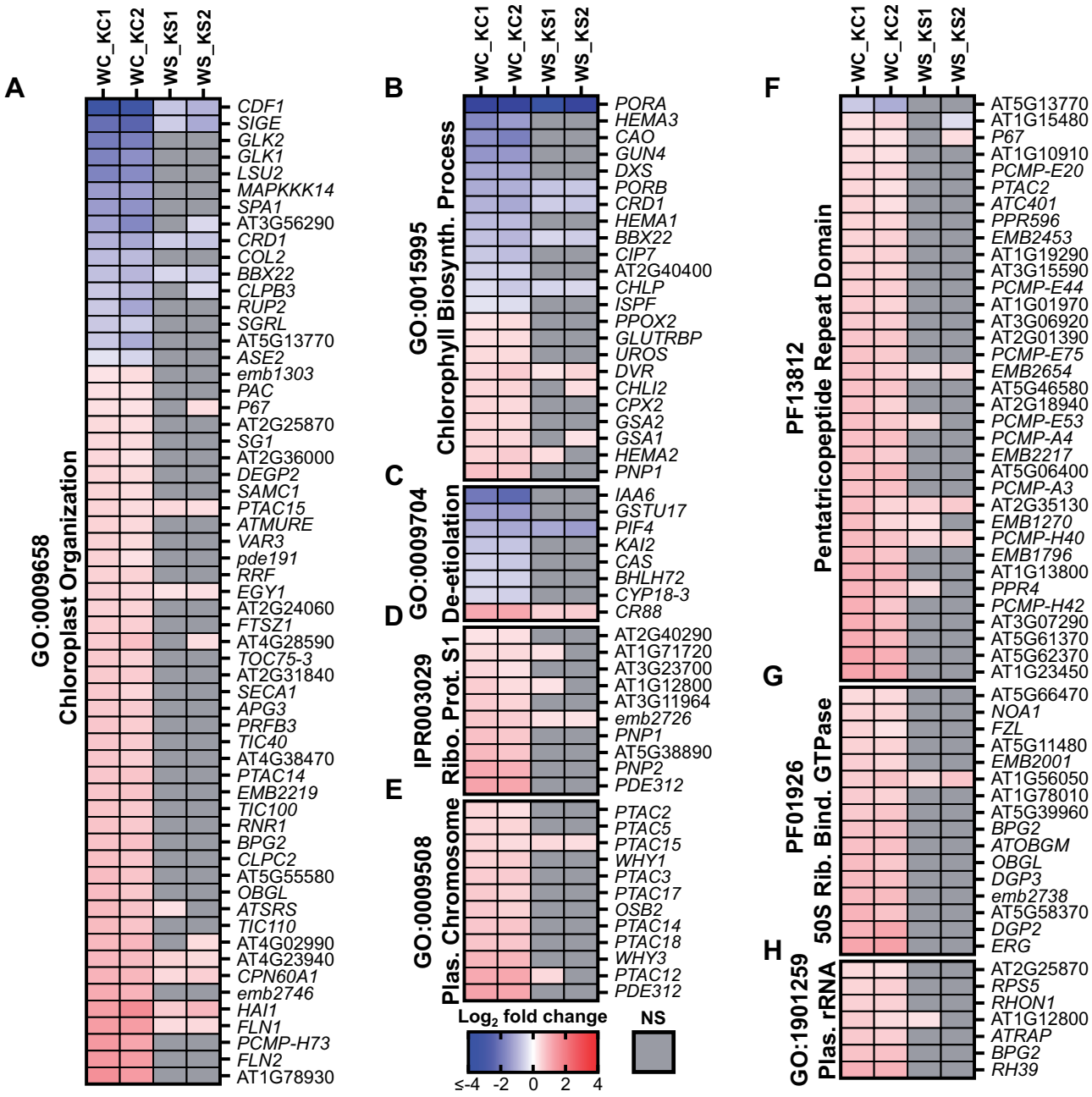

Figure 3 Log_2 fold change expression of individual genes that are significantly differentially expressed in *kea1 kea2* compared with WT under control conditions are no longer differentially expressed when comparing *kea1 kea2* and WT when both are treated with NaCl. A–H, Log_2 fold change gene expression for significantly differentially expressed genes (FDR-adjusted $P < 0.05$) from the WT versus the two independent *kea1 kea2* T-DNA loss-of-function lines under control conditions (WC_KC1 and WC_KC2 for comparisons with *kea1-1 kea2-1* and *kea1-2 kea2-2*, respectively) and corresponding information for the NaCl treatment (WS_KS1 and WS_KS2 for respective *kea1 kea2* lines). Control and NaCl treatments are as described for Figure 1. Red boxes denote statistically significant upregulation; blue boxes denote statistically significant downregulation. Deeper colors represent more extreme changes in log_2 fold change gene expression (see scale bar). Gray boxes denote gene is not significantly differentially expressed (NS, FDR-adjusted $P \geq 0.05$). Annotations include (A) GO term GO:0009658 chloroplast organization; (B) GO term GO:0015995 chlorophyll biosynthetic process; (C) GO term GO:0009704 de-etiolation; (D) INTERPRO domain IPR003029 Ribosomal protein S1, RNA binding domain; (E) GO term GO:0009508 plastid chromosome; (F) PFAM family PF13812 pentatricopeptide repeat domain; (G) PFAM family PF01926 50S ribosome-binding GTPase; (H) GO:1901259 plastid rRNA processing.

annotations included light-harvesting complex (GO:0030076; Supplemental Figure S6A), red and far-red (R/FR) light signaling (GO:0010017; Supplemental Figure S6B), and circadian rhythm (GO:0007623; Supplemental Figure S6D). For each of these GO terms, most transcripts were downregulated under control treatment. However, salt treatment returned expression to WT level as described above. Independent of the FUNC-E analysis, we hand-curated a gene list for the TOC/TIC translocon, which

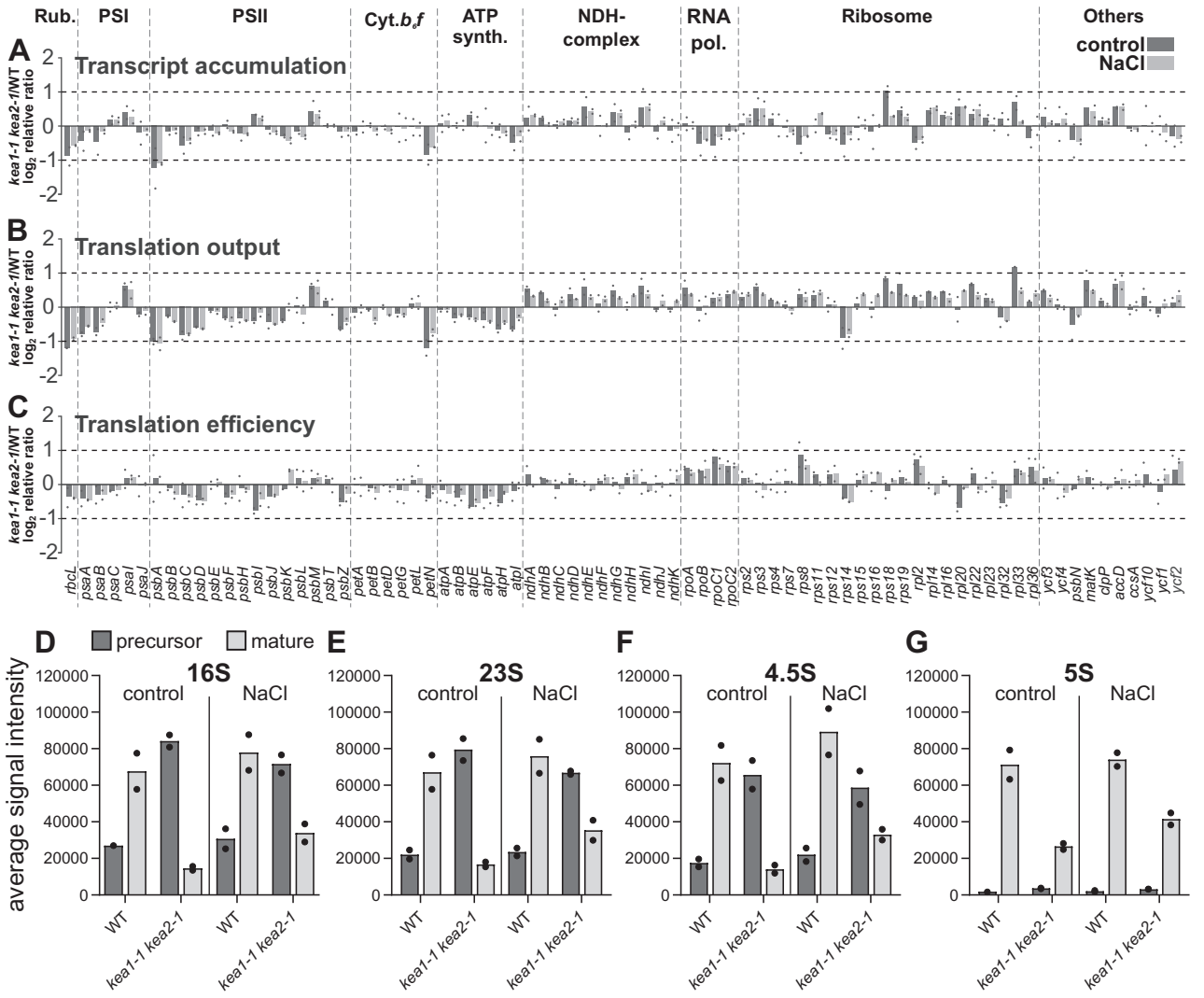

Figure 4 Average transcript accumulation, translation output and translation efficiency of *kea1 kea2* compared with WT show no substantial changes for specific plastid genes under NaCl stress versus control conditions. Detection of a plastid rRNA processing defects in *kea1 kea2*. A The ratio of transcript accumulation, (B) translation output (ribosome footprint abundances), and (C) translation efficiency (ribosome footprint abundances normalized to transcript accumulation) of all chloroplast reading frames is shown as $\log_2$ fold change ratio *kea1-1 kea2-1* versus WT for both control (dark gray bars) and NaCl-treated plants (light gray bars). Control and NaCl treatments are as described for Figure 1. Positive or negative values depict a relative increase or decrease in expression in *kea1-1 kea2-1* relative to WT (average values of $n = 2$; gray dots represent individual biological replicates). The horizontal dotted line indicates less than two-fold change. The dashed vertical lines separate genes according to the complexes their protein products reside in: Rub. = Rubisco, PSI = Photosystem I, , Cyt.b_6f = Cytochrome b_6f complex, ATP synth. = ATP synthase, RNA pol. = RNA polymerase, Others = other proteins. D–G Average signal intensity of (D) 16S, (E) 23S, (F) 4.5S, (G) 5S plastid rRNA transcripts in the WT and *kea1-1 kea2-1* under control and NaCl conditions. Dark gray bars represent signal from the 5′- and 3′-noncoding regions of precursor transcripts, and the light gray bars represent signal from the coding portion of the rRNA transcript. The bars are the average values of $n = 2$; the black dots represent individual biological replicates.

facilitates plastid protein import, a process highly relevant for organelle biogenesis and PGE (Jarvis and Soll, 2001; Köhler et al., 2016). Most transcripts in this category were significantly upregulated in the mutant under control conditions (Supplemental Figure S6C).

In summary, expression analysis of nuclear DEGs and their broad recovery in NaCl-treated mutants substantiated the salt-induced phenotypic rescue reported for *kea1 kea2* double mutants (Kunz et al., 2014). More importantly, it revealed a potential link between plastid ion transport and PGE that may explain the delayed greening phenotype in *kea1kea2*.

Simultaneous loss of KEA1 and KEA2 affects chloroplast rRNA maturation

Intact PGE is a prerequisite for chloroplast development, integrity, and function (Pogson and Albrecht, 2011; Börner et al., 2015). The upregulation of plastid RNA and ribosome-binding proteins uncovered in the RNA sequencing (RNA-SEQ) experiment suggested that PGE might be impacted in

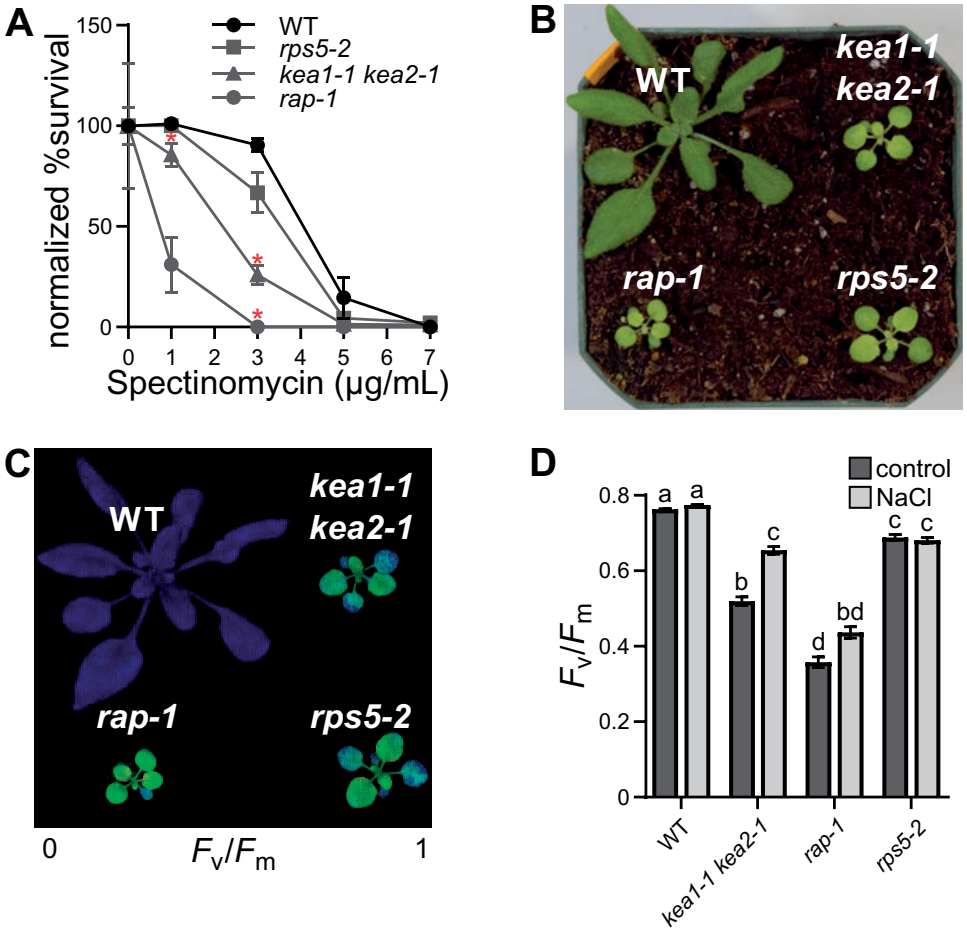

Figure 5 Loss-of-function lines with plastid rRNA maturation defects resemble *kea1 kea2*. A, Percent survival rates for WT, *kea1-1 kea2-1*, *rap-1*, and *rps5-2* phenocopies on increasing concentrations of plastid translation inhibitor spectinomycin (±SEM, $n = 9–10$). Asterisks denote concentration where mean survival rate is significantly below WT survival based on a Kruskal–Wallis test with Dunn's multiple comparisons test for nonparametric data ($P < 0.05$). B, RGB image of WT, *kea1-1 kea2-1*, and phenocopies *rps5-2* and *rap-1*. C, False color image of image of maximum quantum yield of PSII (F_v/F_m) for soil-grown plants. D, Plot of F_v/F_m for ½ MS grown plants with or without NaCl (±SEM, $n = 51–94$). Control (dark gray bars) and NaCl treatments (light gray bars) are as described for Figure 1. Different letters denote significantly different means based on a Kruskal–Wallis test with Dunn's multiple comparisons test for nonparametric data ($P < 0.05$).

kea1 kea2 loss-of-function mutants. Therefore, we investigated if disturbances in K^+/H^+ exchange across the chloroplast envelope caused by simultaneous loss of *KEA1/KEA2* affect PGE. This was achieved by analyzing chloroplast mRNA accumulation and translation by transcript and ribosome profiling with a plastid microarray (Zoschke et al., 2013; Trösch et al., 2018). As in the salt-rescue experiment described previously (Figure 1), we compared chloroplast gene expression from *kea1-1kea2-1* and the WT under control and salt treatment (Figure 4). We were able to document some alterations in transcript accumulation (Figure 4A), translation output (footprint abundances, Figure 4B), and translation efficiency (ribosome footprint abundances normalized to transcript abundances; Figure 4C) in *kea1 kea2* compared with the WT. However, for most genes, the fold change was low, i.e. less than two (ocher-shaded areas in Figure 4; Supplemental Dataset 1). More importantly, not a single chloroplast gene exhibited substantially altered expression between *kea1 kea2* and WT comparing salt treatment and control condition (i.e. more than two-fold change). Altogether, the mild changes in the transcript accumulation of specific chloroplast genes are an unlikely cause for the observed phenotypic differences between salt and control conditions. This contrasts our observations on alterations in nuclear gene expression (Figures 2 and 3; Supplemental Figure S6).

The probes on the chloroplast microarray also allow for semi-quantitative estimation of the rRNA-processing status, although the high abundance of mature rRNAs and concomitant saturation effects may skew these estimations. Nevertheless, we noticed unusually high-signal intensities from probes covering 5′- and 3′-immature extensions of 16S (Figure 4D), 23S (Figure 4E), and 4.5S (Figure 4F) but not 5S rRNAs (Figure 4G) in *kea1 kea2* control samples. The probe signals for the mature portions of the aforementioned rRNAs in *kea1 kea2* were reduced. Typically, 5′- and 3′-regions give lower signals, as seen in the WT, because they are cleaved during rRNA maturation (Manavski et al.,

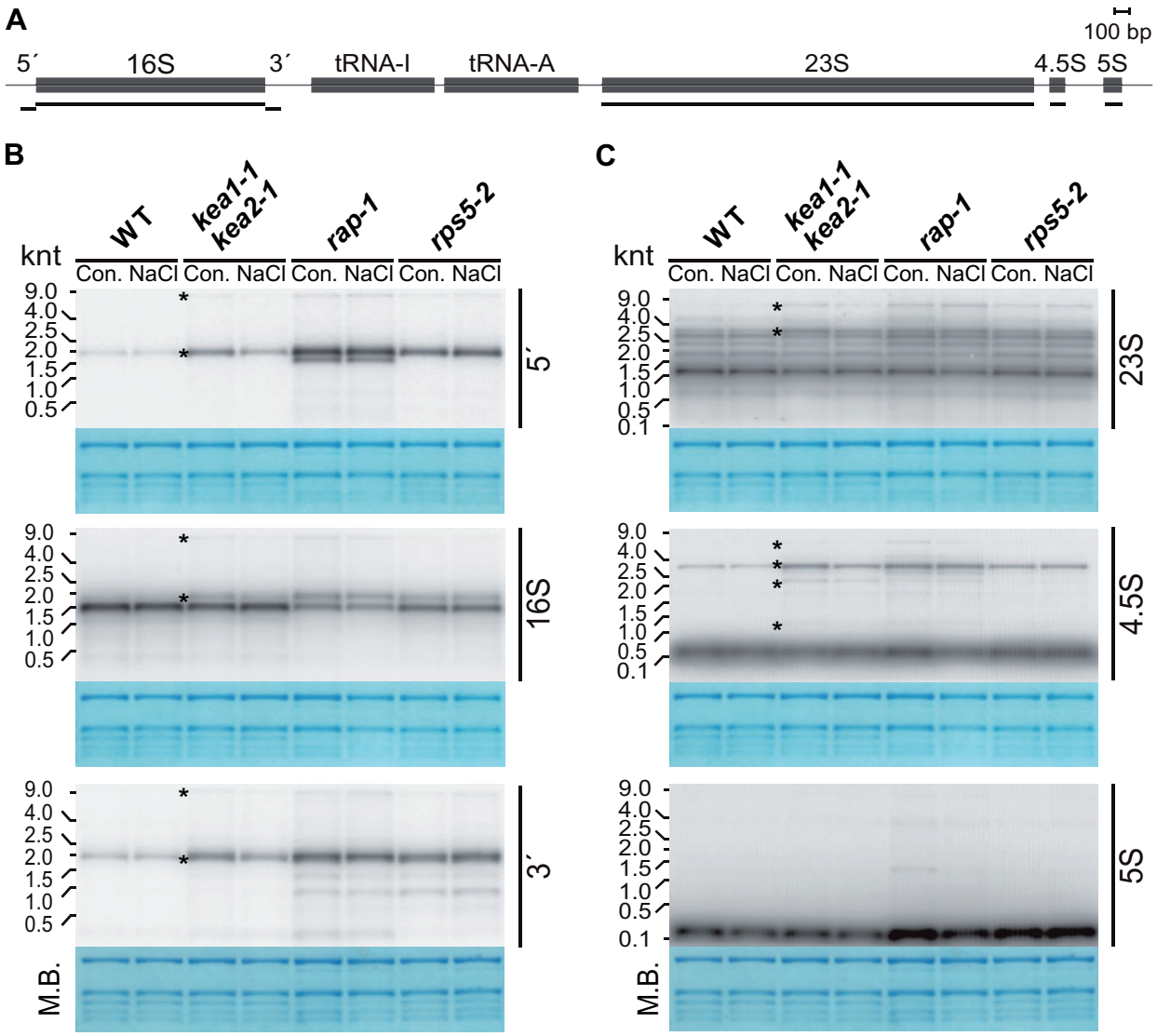

Figure 6 Plastid rRNA processing defects in the *kea1 kea2* mutant are alleviated under NaCl stress conditions compared with control conditions. A, Physical map of the plastid rRNA transcript with binding position of probes (black lines) used in RNA gel blot analyses. B, From top to bottom: RNA gel blot analyses of 16S rRNA accumulation using probes against the 5′-noncoding region (5′), the 16S rRNA coding region (16S), and the 3′-noncoding region (3′). In the middle blot, the upper and lower bands represent unprocessed and mature 16S rRNA, respectively. C, The same RNA gel blots from (B) rehybridized to analyze additional plastid rRNAs. From top to bottom: 23S, 4.5S, and 5S rRNA accumulation. Sizes of marker bands are indicated on the left side in kilonucleotides (knt). Pictures of methylene blue-stained chloroplast and cytosolic rRNAs (M.B.) are provided below each blot to illustrate equal loading. Black asterisks show the rRNA precursor bands whose accumulation changes in *kea1-1 kea2-1* upon NaCl treatment. Samples analyzed include control and NaCl-treated WT, *kea1-1 kea2-1*, and two lines with previously characterized plastid rRNA maturation defects, *rap-1* and *rps5-2*. Control and NaCl treatments are as described for Figure 1.

2018). Salt treatment resulted in signal reductions from the immature extensions and moderate increases in signal from the functional mature regions in *kea1 kea2* compared with WT. Hence, our results suggest a disturbed rRNA maturation in *kea1kea2*.

To further investigate the potential rRNA processing effect, we compared the phenotype of *kea1-1kea2-1* with two previously described mutants: *rap-1* (Kleinknecht et al., 2014) and *rps5-2* (Figure 5; Zhang et al., 2016). In both mutants, the loss of a cRBP results in a chloroplast rRNA maturation defect. To test disruption of chloroplast rRNA function, we subjected all three mutants to increasing concentrations of spectinomycin, which binds bacterial ribosomes and inhibits translation (Brink et al., 1994). All three mutant lines were more susceptible to the inhibitor than the WT, indicating a preexisting deficit of functional ribosomes (Figure 5A). The *rap-1* mutant was the most sensitive (survival rate <50% at 1 μg ml^{-1}), *rps5-2* was the least sensitive (survival rate <50% at 5 μg ml^{-1}), and *kea1-1kea2-1* had an intermediate susceptibility (survival rate <50% at 3 μg ml^{-1}). When we grew *kea1-1kea2-1*, *rap-1*, and *rps5-2* side-by-side, all three mutants displayed a delayed-greening phenotype with pale young leaves, which improved with leaf age (Figure 5B). F_v/F_m was significantly lower in young

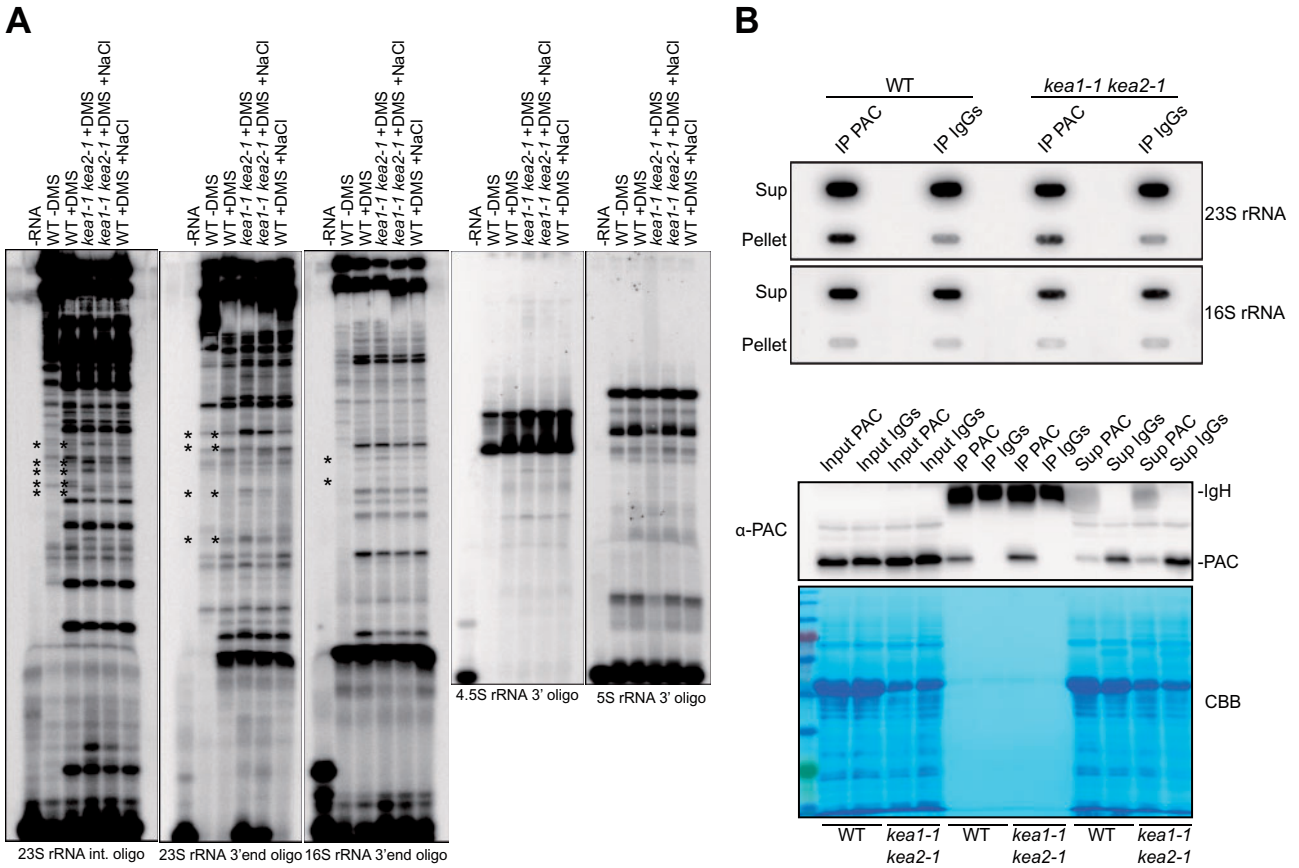

Figure 7 Plastid ribosomal RNA structures and protein RNA binding are affected in *kea1 kea2* plants. A, Leaf tissue was DMS-treated, and then, RNA was extracted and used in a radiolabeled primer extension assay to probe secondary RNA structure of all plastid rRNA transcripts. Untreated leaf RNA (WT-DMS) served as negative control. Fragments present across all lanes represent reverse transcription abortion products originating from general RNA secondary structures or processing sites. Bands occurring only in DMS-treated samples correspond to methylation events in unstructured or free-of-protein RNA segments. Differences between DMS-treated WT, *kea1-1-kea2-1*, and NaCl-treated *kea1-1 kea2-1* samples are marked with asterisks. Control and NaCl treatments are as described for Figure 1. Strong effects found in 23S rRNA are denoted by two asterisks. B, Co-IP analysis of PALE CRESS (PAC) protein shows reduced binding (24.3% ± 1.2 SEM, $n = 3$) to its target the 23S rRNA in *kea1-1 kea2-1* compared with WT. SDS–PAGE and immunoblot show efficiency of co-IPs. (Upper) Slot blot hybridization of RNA associated with PAC, (lower) immunodetection of immunoprecipitated PAC protein. IP, immunoprecipitation; Sup, supernatant; IgGs, control IgGs that do not recognize PAC; IgH, immunoglobulin heavy chain; CBB, Coomassie Brilliant Blue. A representative result of three replicates is shown for both (A) and (B).

leaves of all three mutants (Figure 5C). Again, the phenotype was most extreme in *rap-1*, while *rps5-2* was less affected than the *kea1-1kea2-1* mutant. Interestingly, *kea1-1kea2-1* recovered in the presence of NaCl, yet neither *rap-1* nor *rps5-2* showed a significant F_v/F_m increase, although a slight, non-significant F_v/F_m increase was noticeable in *rap-1* (Figure 5D).

Next, we carried out RNA gel blots to probe all four plastid rRNA species (Figure 6). In the case of the 16S rRNA, three different probes were hybridized: functional transcript, 5′-extension transcript, and 3′-extension transcript. For 23S, 4.5S, and 5S rRNAs, the functional transcript regions were probed (Figure 6A). Substantiating the microarray results (Figure 4, D–F), we found unprocessed 16S, 23S, and 4.5S rRNA transcripts to accumulate in *kea1 kea2* under control conditions (Figure 6, B and C). A similar albeit more severe maturation defect was found in control *rap-1* and *rps5-2* plants (Figure 6, B and C). Interestingly, NaCl treatment reduced the accumulation of immature 16S, 23S, and 4.5S RNAs in *kea1 kea2* (Figure 6, B and C) but had no effect on rRNA maturation in *rap-1* or *rps5-2* (Figure 6, B and C). The maturation of 5S rRNA transcripts was similar across genotypes regardless of the treatment. In summary, the virescent phenotype in *kea1 kea2* is associated with rRNA processing defects, which are rescued by NaCl exposure.

The secondary structure of plastid rRNA transcripts and RNA–protein interactions are compromised in *kea1 kea2* mutants

RNA processing relies on direct interaction between transcript and cRBPs (Stoppel and Meurer, 2011; Barkan and Small, 2014). These interactions are dependent on the secondary structure of transcripts. Therefore, we performed dimethyl sulfate (DMS) treatments to test if the *in vivo* structure of rRNA transcripts is altered when the two envelope K^+/H^+ exchangers are missing. DMS, a readily diffusible

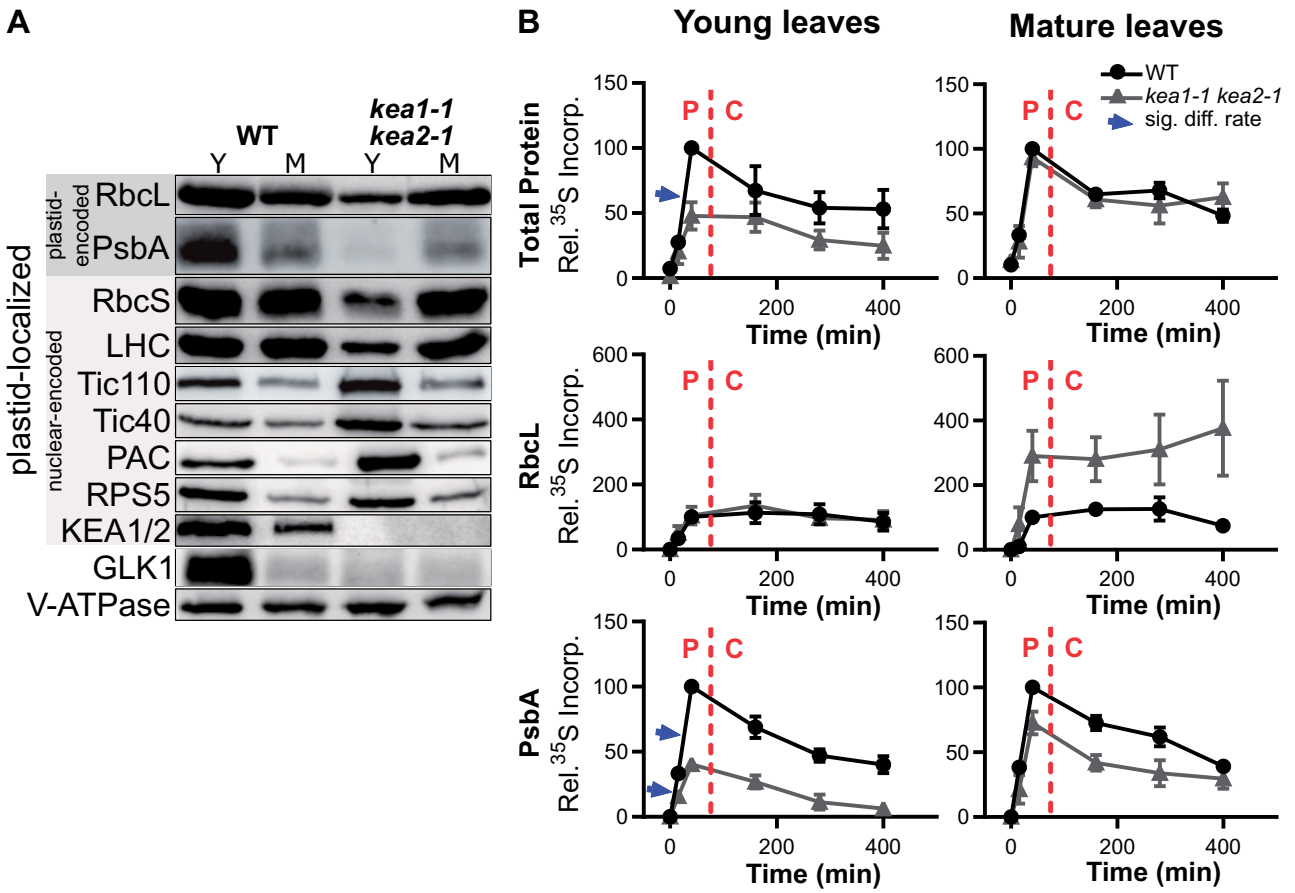

Figure 8 Immunoblots and pulse-chase experiments revealed lower steady-state levels of plastid-encoded proteins, and decreased translation rates. A, B, All experiments carried out in young (Y) versus mature (M) leaf tissue from WT and *kea1-1 kea2-1*. A, Immunoblots for steady-state levels of plastid and nuclear-encoded proteins. Plastid-encoded proteins include Rubisco large subunit (RbcL) and the D1 reaction center of PSII (PsbA). Nuclear-encoded plastid-targeted proteins include Rubisco small subunit (RbcS), LHC a/b binding protein, protein import complex components Tic110 and Tic40, chloroplast rRNA binding protein Pale Cress (PAC), plastid ribosomal protein S5 (RPS5), and K^+/H^+ antiporters KEA1/KEA2. The nuclear-targeted transcription factor involved in PhANG expression Golden-Like 1 (GLK1) was also quantified. Vacuolar ATPase (V-ATPase) was used to probe the abundance of non-chloroplast proteins and demonstrate equal loading of samples. Additional blot is shown in Supplemental Figure S8. B, Quantification of total protein produced in pulse-chase experiment (top), RbcL production (middle), and PsbA (bottom). Leaf discs were harvested after 0, 15, and 40 min during the pulse portion of the experiment. After chase with nonradioactive amino acids, samples were taken every 2 h for a total of 400 min. Red line represents transition from pulse (P) to chase (C) stage. For each parameter, values were normalized to the intensity of the WT at the 40-min timepoint for each leaf age (±SEM, $n = 3$). Blue arrows adjacent to line indicate *kea1-1 kea2-1* has a significantly lower protein synthesis rate from the WT at given timepoint based on an ordinary two-way ANOVA with Šídák's multiple comparisons test ($P < 0.05$). Images of the autoradiographs are available in Supplemental Figure S9.

reactive reagent, methylates adenine and cytosine bases exclusively in single-stranded RNAs. DMS methylation of nucleotides prevents base pairing during a reverse transcription primer extension assay, resulting in shorter primer extension products. Less structured transcripts that are unprotected through protein binding have higher DMS reactivity and thus yield altered patterns of extension products. Indeed, we observed significant and highly reproducible structural changes in *kea1 kea2* in 23S transcripts and mild changes in 16S rRNA transcripts (Figure 7A). Structural alterations were less prevalent when mutant plants were grown in the presence of NaCl.

The structural RNA changes may affect the capacity of cRBPs to bind their target. This could explain the observed processing defects in 16S, 23S, and 4.5S rRNAs. As most chloroplast RNA-binding proteins are encoded in the nucleus (Barkan, 2011; Manavski et al., 2018), we initially tested if the lack of KEA1 and KEA2 hampers protein import into the organelle. The uptake rates for two well-established import substrates, ferredoxin-$NADP^+$ reductase (FNR), and pyruvate dehydrogenase E1 alpha subunit (E1α) into isolated *kea1 kea2* mutant plastids were no different from WT (Supplemental Figure S7). Therefore, the rRNA processing defects documented in *kea1 kea2* are not caused by a shortage of nuclear-encoded cRBPs in the chloroplast. Next, we tested RNA–protein interaction via RNA-Co-IP between the PALE CRESS (PAC) protein and one of its specific binding targets, the 23S rRNA transcript (Meurer et al., 2017). Even though slightly more PAC was immunoprecipitated in mutant specimens, the amount of bound 23S rRNA was

reduced by 24.3% (±1.2 SEM, $n = 3$) in *kea1 kea2* compared with WT PAC isolates (Figure 7B).

Steady-state levels of plastome-encoded proteins are reduced in *kea1 kea2* mutants

To investigate if the documented disruptions of rRNA metabolism impact the chloroplast proteome at different leaf developmental stages, we compared the steady-state level of selected nuclear- and plastome-encoded proteins in *kea1 kea2* young pale leaves and mature green leaves with respective WT tissues (Figure 8A; Supplemental Figure S8). Initially, we checked protein levels of the vacuolar–ATPase as a loading control. V-ATPase amounts were unchanged between genotypes and leaves of different ages. KEA1 and KEA2 carriers were more abundant in young WT leaves, but as expected were absent from *kea1 kea2* protein extracts. Interestingly, plastome-encoded Rubisco small subunit (RbcL) and PsbA proteins were markedly decreased in young pale *kea1 kea2* leaf tissue compared with young WT tissue. However, RbcL was detectable at WT levels in the older green leaves of *kea1 kea2*. The two PhANG-encoded proteins Rubisco small subunit (RbcS) and light harvesting chlorophyll (LHC) were decreased in *kea1 kea2* young leaves but present at WT level in older tissue. Correspondingly, GLK1, the TF controlling PhANG expression (Waters et al., 2009) was barely detectable in *kea1 kea2* young leaves but very pronounced in WT young leaves. Finally, the plastid protein translocon subunits Tic110 and Tic40 and the two tested cRBPs, RPS5, and PAC, were more abundant in *kea1 kea2* young leaves than in corresponding WT tissue.

Pulse-chase studies reveal altered translation in kea1 kea2 chloroplasts

The ribosome profiling method is useful to unveil translation defects for specific chloroplast genes. However, the rRNA processing defect in *kea1 kea2* may cause a general chloroplast translation deficiency as indicated by altered steady-state levels of plastome-encoded proteins (Figure 8A; Supplemental Figure S8). These global differences may become obscured by normalization in ribosome profiling. Hence, we performed pulse-chase assays to determine if in *kea1 kea2* the overall synthesis or turnover of plastome-encoded proteins was altered due to translational defects. In consideration of the characteristic delayed greening phenotype in *kea1 kea2*, we again investigated young and mature leaves from both genotypes separately (Figure 8B; Supplemental Figure S9). Initially, we analyzed total chloroplast translation and protein turnover rates in young and mature leaf samples under illumination. The pulse portion of the experiment revealed significantly lower rates of ^{35}S incorporation in *kea1 kea2* chloroplast proteins compared with WT specifically in young leaves (Figure 8B). Protein degradation rates did not vary significantly over the course of the 320-min chase period. RbcL and PsbA, the two most abundantly synthesized proteins in chloroplasts, were utilized to track the translation degradation kinetic of individual proteins. Unexpectedly, RbcL translation occurred to the same degree in young WT and *kea1 kea2* leaf tissue, and yet older green *kea1 kea2* leaves showed a significant increase of RbcL synthesis compared with its respective WT control tissue. RbcL protein was also very stable and no significant loss in labeling was detected in either genotype during the chase portion of the assay. In contrast, PsbA synthesis rates were strongly reduced in young pale *kea1 kea2* leaves. The difference between the genotypes was less dramatic in older leaves. As expected, PsbA turnover was quick and took place at a similar rate in WT and *kea1 kea2* during the 320-min-long chase period. We conclude that overall chloroplast protein production rates are lower in *kea1 kea2*. This effect is most dramatic in the pale young mutant leaf tissue.

Immature rRNAs in kea1 kea2 affect polysome loading

We have documented structural changes in rRNA transcripts, reduced RNA-protein binding, buildup of unprocessed rRNAs, and lower protein output in *kea1 kea2* chloroplasts. Thus, we hypothesized that immature rRNAs in mutants may not properly assemble into functional plastid ribosomes. To test this hypothesis, we fractionated polysomes in sucrose gradients and probed specific transcripts in addition to 16S and 23S rRNAs. We observed a clear shift toward lower density fractions (lower numbers) for all probed RNAs in *kea1 kea2* under control conditions (Figure 9A). This finding indicates that in mutants fewer ribosomes were bound to plastome mRNAs explaining in part the reduced chloroplast translation rate and lower steady-state level of plastome-encoded proteins (Figure 8). When *kea1 kea2* plants were grown in the presence of NaCl the distribution of polysome-bound RNAs more closely resembled WT as we found stronger signals in higher density fractions (higher numbers) for all RNA probes (Figure 9B). This implies that ribosome loading onto mRNAs recovered in NaCl-treated *kea1 kea2*. In parallel, we extracted total leaf proteins from all specimens. Immunoblotting confirmed that steady-state levels of plastome-encoded proteins represented by RbcL and PsbA were reduced in the *kea1-1kea2-1* mutants under control conditions but increased upon NaCl treatment (Figure 9C). In line with the recovery of photosynthetic parameters (Figure 1), protein amounts of the two PhANGs RbcS and LHC also recovered in NaCl-treated *kea1 kea2* plants.

The GUN1-dependent RS pathway acts to suppress the GLK1/GLK2 nexus in kea1 kea2 mutants

Our transcriptomics data showed that the *GLK1/GLK2* TFs responsible for chloroplast development and PhANG expression were downregulated in *kea1 kea2* under control conditions (Figure 3A; GO:0009658 chloroplast organization). Consequently, GLK1 protein did not accumulate in young mutant leaves (Figure 8A). The GLK1/GLK2 downstream

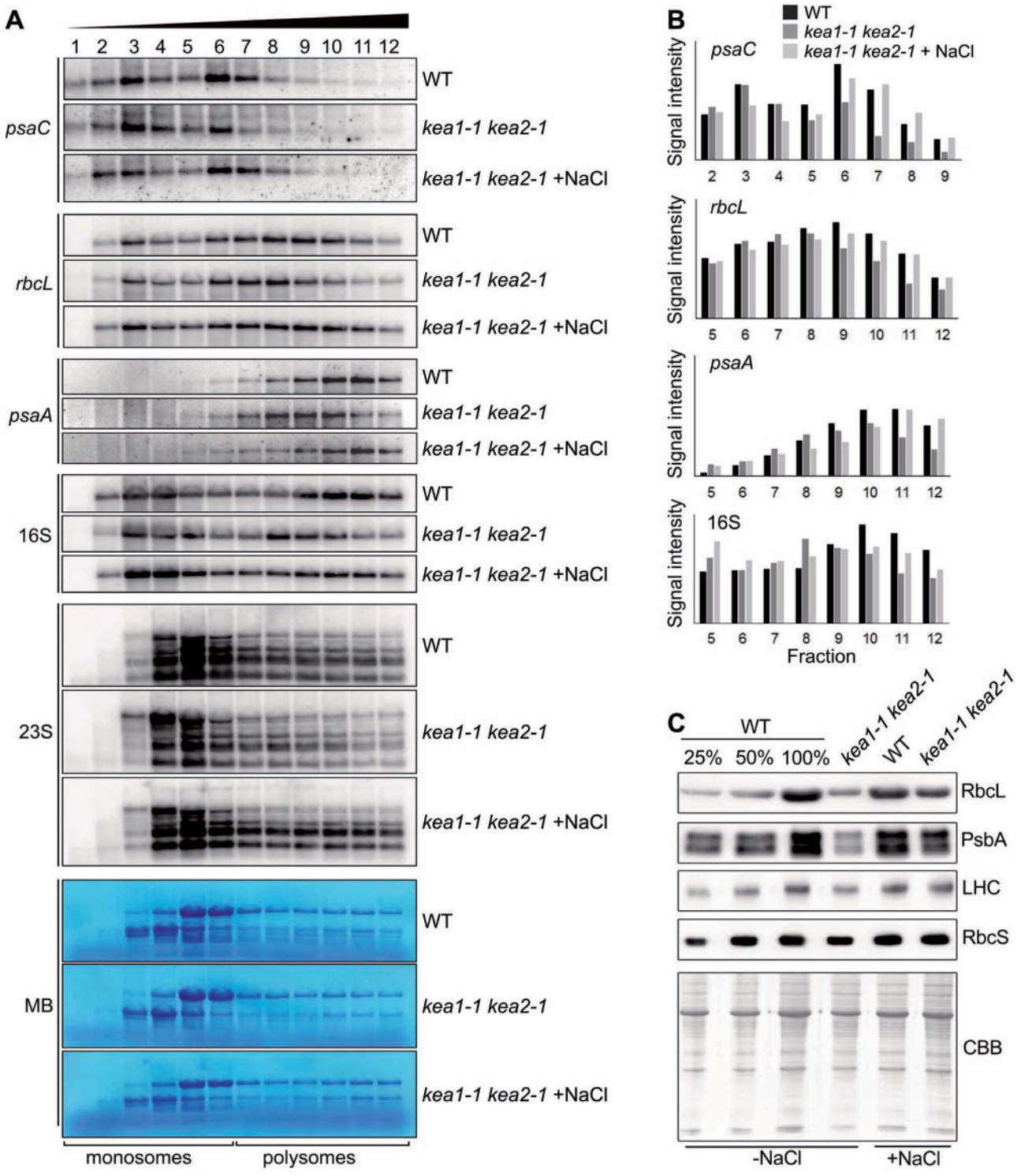

Figure 9 Polysome loading and immunoblot analysis of chloroplast proteins showing recovered PGE in NaCl-treated *kea1 kea2* plants. A, Polysomes were isolated via sucrose density gradients and fractions probed via RNA blot for loading with *psaC*, *rbcL*, and *psaA* mRNAs and 16S or 23S rRNAs, respectively. Increasing fraction numbers represent heavier polysomes. A representative result of three replicates is shown. MB = methylene blue staining. B, Quantification of transcript abundance from (A) showed more similar polysome loading to WT if *kea1 kea2* was treated with NaCl. NaCl treatments are as described for Figure 1. C, Immunoblotting of total protein extracts from same plant tissue showed higher steady-state protein levels for plastome-encoded proteins RbcL and PsbA, and for nuclear-encoded PhANGs LHC and RbcS in NaCl-treated *kea1-1 kea2-1*. CBB, Coomassie Brilliant Blue.

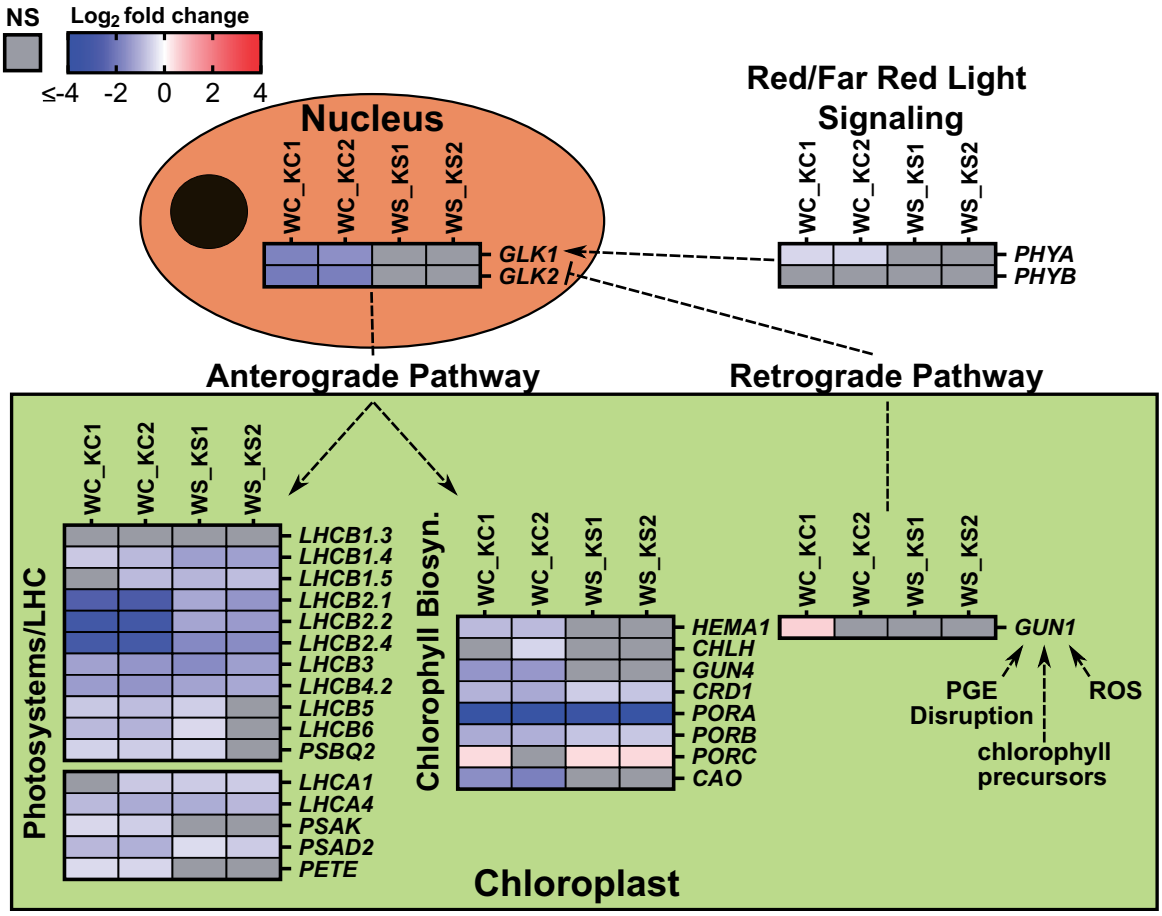

Figure 10 Expression of GLK1/GLK2 transcription factors and downstream PhANGs is suppressed in *kea1 kea2* compared with the WT but recovers under NaCl treatment. A, Log_2 fold change values of *GLK1/GLK2* and downstream target genes when comparing the WT to two independent *kea1 kea2* lines under control conditions (WC_KC1 and WC_KC2 for comparisons with *kea1-1 kea2-1* and *kea1-2 kea2-2*, respectively) and NaCl treatment (WS_KS1 and WS_KS2 for comparisons with *kea1-1 kea2-1* and *kea1-2 kea2-2*, respectively). NaCl treatments are as described for Figure 1. Red boxes denote statistically significant upregulation; blue boxes denote statistically significant downregulation (FDR-adjusted $P < 0.05$). Deeper colors represent more extreme changes in log_2 fold change gene expression (see scale bar). Gray boxes denote gene is not significantly differentially expressed (NS, FDR-adjusted $P \geq 0.05$).

targets have been well characterized to contain numerous PhANGs, particularly LHC components and chlorophyll biosynthesis enzymes (Fitter et al., 2002; Waters et al., 2009; Berry et al., 2013). We used the gene information to draw a quantitative GLK1/GLK2 nexus map by plotting RNA-SEQ log_2 fold change values from our WC_KC and WS_KS comparisons (Figure 10). Indeed, we found that GLK1/GLK2 and many of their downstream targets were significantly downregulated in the *kea1 kea2* mutant under control conditions but were no longer significant upon salt treatment (Figure 10). This suggests PhANG suppression via reduction of *GLK1/GLK2* transcripts in *kea1 kea2* is a response to disturbed plastid ion transport and contributes to the low content of chlorophyll and photosynthetic rates found in the mutant. Negative regulation of *GLK1/GLK2* and subsequent PhANG suppression was shown to delay chloroplast development (Fitter et al., 2002; Waters et al., 2009), and has been suggested as a coping mechanism to minimize damage in malfunctioning plastids (Kakizaki et al., 2009; Leister and Kleine, 2016).

This raises the question of how chloroplasts can sense and communicate ion imbalance to the nucleus to trigger changes in gene expression via GLK1/GLK2 TFs. Two main pathways control GLK1/GLK2 transcription: (1) R/FR light signaling via phytochromes activates *GLK1/GLK2* expression (Waters et al., 2008; Oh and Montgomery, 2014) and (2) the chloroplast-to-nucleus RS pathway suppresses specifically *GLK1* transcription through function of its central player GENOMES UNCOUPLED 1 (GUN1) (Kakizaki et al., 2009; Waters et al., 2009; Martin et al., 2016). Consequently, we investigated both pathways in the *kea1 kea2* background to uncover which pathway is involved in the response to loss of envelope K^+/H^+ exchange and the resulting negative effects on PGE. Based on RNA-SEQ data, neither the R/FR-sensing phytochromes *PHYA/PHYB* nor the RS component *GUN1* exhibit dramatic alteration of transcript levels (Figure 10). However, our FUNC-E analysis showed that downstream components of R/FR light perception (GO:0010017; Supplemental Figure S6, B) were enriched in our RNA-SEQ dataset.

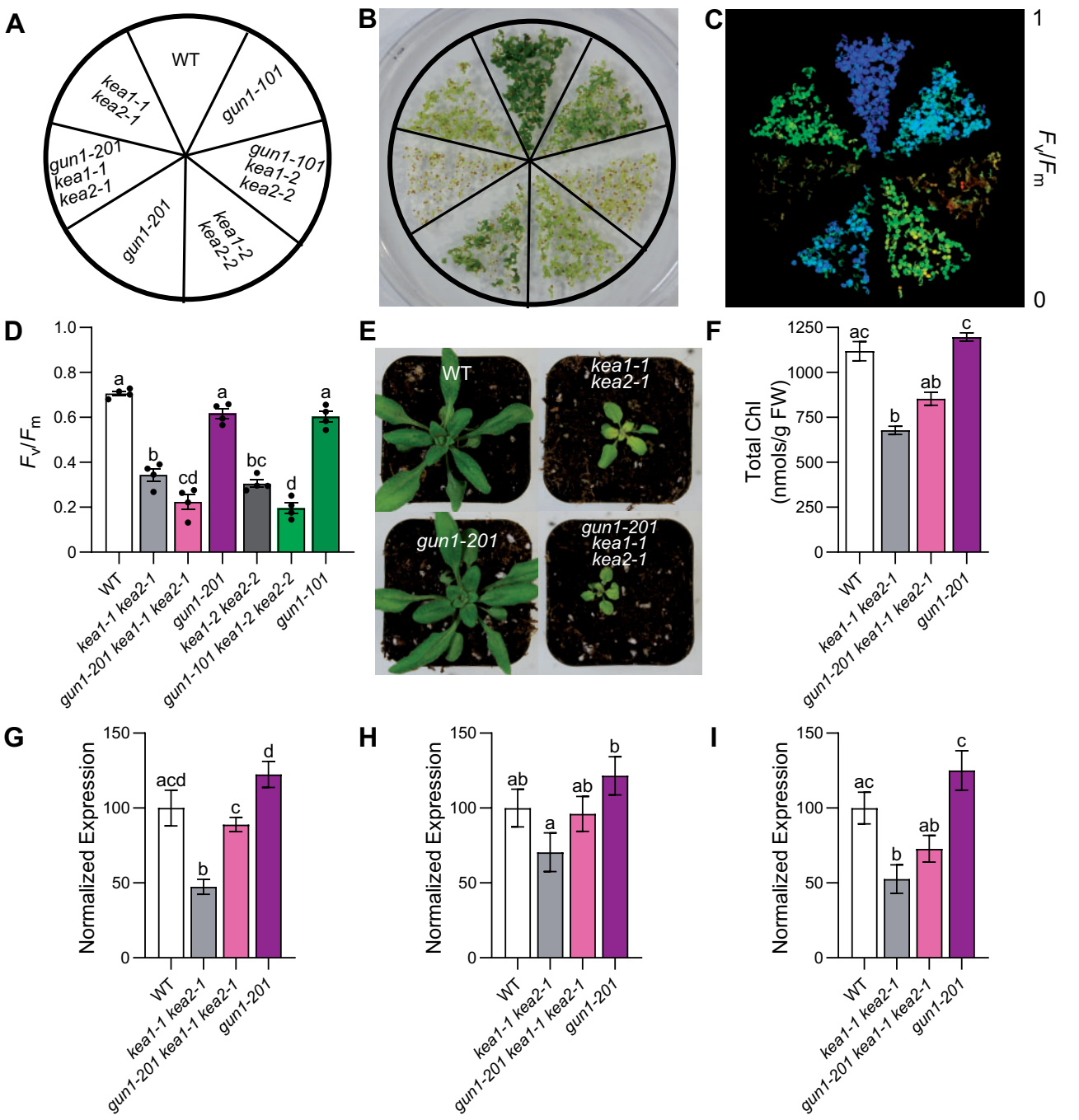

Figure 11 Retrograde signaling via GUN1 is triggered in response to loss of KEA1/KEA2 to downregulate PhANGs. A, Schematic showing genotype position on the plate. B, RGB and (C) false color image of maximum quantum yield of PSII (F_v/F_m) of 1-week-old plants including WT, two independent *gun1* loss-of-function mutants, the two independent *kea1 kea2* mutants, and *gun1 kea1 kea2* triple mutants. D, Mean F_v/F_m for 1-week old seedlings in Figure 11C (±SEM, $n = 4$, points represent individual bioreplicates). Different letters above the bars denote significantly different means based on an ordinary 1-way ANOVA with Tukey's multiple comparisons test ($P < 0.05$). E, Three-week-old plants including WT, *kea1-1 kea2-1*, *gun1-201*, and *gun1-201 kea1-1 kea2-1* mutant. F, Total chlorophyll content of three-week-old plants from Figure 10E (±SEM, $n = 12$). Different letters above the bars denote significantly different means based on a Kruskal–Wallis test with Dunn's multiple comparisons test for nonparametric data ($P < 0.05$). G–I, Normalized gene expression based on RT-qPCR in three-week-old WT, *gun1-201*, *kea1-1 kea2-1*, and *gun1-201 kea1-1 kea2-1* lines (±SEM, $n = 8–9$). Genes tested included GLK1 (H), LHCB1.2 (I), and LHCB2.2 (J). Different letters above the bars denote significantly different means based on either an ordinary one-way ANOVA with Tukey's multiple comparisons test for normally distributed data, or a Kruskal–Wallis test with Dunn's multiple comparisons test for nonparametric data ($P < 0.05$).

Therefore, we set up germination experiments under monochromatic R/FR light and determined the hypocotyl length as a proxy for R/FR light signal perception (Fukazawa et al., 2020). As positive controls, we included phytochrome-deficient mutants *phyb* in red light or *phyA* for FR light experiments, respectively (Nagatani et al., 1993; Reed et al., 1993; Neff and Chory, 1998). The *kea1 kea2* hypocotyl length under both monochromatic light treatments was roughly the same as in WT when normalized to a dark-grown control (Supplemental Figure S10). Conversely, *phyb* and *phyA* mutants failed to respond to R/FR light, respectively, and revealed the characteristically extended hypocotyl under the given light condition. Consequently, perturbed R/FR light signaling is unlikely a factor in the observed low *GLK1/GLK2* expression in *kea1 kea2* double mutants.

Disruption of PGE, changes in tetrapyrrole biosynthesis, and reactive oxygen species (ROS) accumulation result in downregulation of the PhANGs via *GLK1* suppression. This occurs through the RS pathway and its main mediator GUN1 (Kleine and Leister, 2016; Hernandez-Verdeja and Strand, 2018; Tadini et al., 2020). We demonstrated that PGE is decreased in *kea1 kea2* mutants (Figures 4–9). Additionally, we documented significantly higher H_2O_2, i.e. ROS production in *kea1 kea2* leaves compared with WT under control conditions (Supplemental Figure S11, A and B). To genetically test the role of the RS pathway in governing *GLK1* expression in response to disturbed plastid ion transport, we introgressed two independent *gun1* T-DNA insertion lines *gun1-101* (Ruckle et al., 2007) and *gun1-201* (Martin et al., 2016) into both *kea1 kea2* lines and isolated *gun1 kea1 kea2* triple mutants (Figure 11).

When we germinated all genotypes side-by-side and documented their photosynthetic capacity. We noticed a strongly aggravated phenotype in both *gun1 kea1 kea2* lines compared with parental mutant lines (Figure 11, A–D). Many *gun1 kea1 kea2* triple mutant seedlings either died immediately after germination or showed significantly lower F_v/F_m than *kea1 kea2* double or *gun1* single mutants. Interestingly, a few *gun1 kea1 kea2* triple mutant individuals did survive. These slow-growing individuals were visibly greener and indeed had increased total chlorophyll compared with *kea1 kea2* (Figure 11, E and F; Supplemental Figure S12). In line with the previously assigned role of GUN1 in the suppression of *GLK1* and the PhANGs (Kakizaki et al., 2009; Waters et al., 2009; Martin et al., 2016), our quantitative PCR data show that *GLK1* mRNA level was suppressed in *kea1 kea2* double mutants compared with the WT, but recovered in *gun1 kea1 kea2* triple mutants (Figure 11G). Furthermore, representative PhANG members downstream of GLK1, namely *LHCB1.2* and *LHCB2.2*, showed closer to WT mRNA levels (Figure 11, H and I). Thus, the increase in chlorophyll in older triple mutants (Figure 11F) is likely due to PhANG expression in the absence of GUN1-mediated GLK1 suppression. We hypothesize that the high rate of *gun1 kea1 kea2* seedling mortality is due to pre-existing oxidative stress exacerbated by uncontrolled expression of the PhANGs after loss of GUN1. Our finding that *kea1 kea2* double mutants exhibit increased levels of plastid H_2O_2 supports this hypothesis (Supplemental Figure S11).

Discussion

In this study, we characterized the consequences resulting from the loss of KEA1/KEA2, two chloroplast envelope K^+/H^+ exchangers, as well as compensatory mechanisms used by the plant cell to tolerate this defect. Previous studies revealed that *kea1 kea2* double mutants exhibit altered chloroplast biogenesis, delayed leaf greening, and impaired photosynthesis (Kunz et al., 2014; Aranda-Sicilia et al., 2016). However, the mechanistic link between loss of transport function and the developmental defects remained unknown (Sze and Chanroj, 2018). Here, we show through a systems biology approach that the delayed chloroplast biogenesis and leaf greening in *kea1 kea2* originate from an impairment of PGE.

Moderate NaCl stress, a treatment known to revert developmental defects in *kea1 kea2* (Kunz et al., 2014), was used in combination with RNA-SEQ to pinpoint regulatory and metabolic pathways most altered by loss of *KEA1/KEA2*. Functional enrichment analysis revealed numerous genes with photosynthesis and chloroplast-related annotations were deregulated in *kea1 kea2* (Figure 2). However, only a small set of these annotation groups recovered to WT levels under NaCl treatment. Most of these annotations were related to chloroplast RNA metabolism. A deeper investigation of these genes revealed that many cRBPs involved in RNA processing and editing were upregulated in *kea1 kea2*, suggesting that a cellular program was triggered to compensate for a defect in the organelle's RNA metabolism or other impairments of PGE (Figure 3).

Through plastid transcriptomics and RNA gel blotting, we documented maturation defects for most chloroplast rRNAs (16S, 23S, and 4.5S) in mutants (Figures 4 and 6). Polysome studies and pulse–chase experiments suggest that this defect impacts the assembly and function of chloroplast ribosomes in *kea1 kea2* chloroplasts (Figures 8 and 9). In young pale leaves, the steady-state levels and translation rates for chloroplast-encoded proteins, especially for PsbA, were drastically decreased. Interestingly, *kea1 kea2* mutants phenotypically resemble "virescent" (pale young leaf) mutants such as *rap* and *rps5*, which both suffer from plastid rRNA maturation defects (Figure 5). All three mutant lines were susceptible to the bacterial ribosome inhibitor spectinomycin, a typical behavior for mutants in which the pool of functional ribosomes is reduced by genetic defects. In summary, our data suggest that *kea1 kea2* null mutants are affected in PGE because of rRNA processing defects.

These findings raise the question: Why are plastid ribosomes impacted by the loss of KEA1/KEA2 and resulting diminished K^+/H^+ exchange across the envelope membrane? PGE relies heavily on nuclear-encoded cRBPs (Barkan, 2011; Hammani et al., 2014; Manavski et al., 2018). Our *in vitro* import assays suggest that protein uptake in *kea1 kea2* mutant

chloroplasts proceeds at WT rates (Supplemental Figure S7). The transcriptomic data revealed a striking increase in nuclear-encoded cRBP transcripts (Figure 3). By immunoblotting two representative cRBPs, RPS5 and PAC, we show that protein and mRNA levels correspond. Therefore, we conclude that sufficient amounts of RNA-binding protein are present in *kea1 kea2* mutant chloroplasts. Hence, the rRNA processing defect exhibited by *kea1 kea2* mutants is likely the result of reduced binding or activity of RNA-binding proteins. *In vitro* studies on cRBP member PPR10 established that the binding capacity of PPR10 to its target mRNA is strongly dependent on electrostatic forces (McDermott et al., 2018). Even weak changes to RNA structure, such as secondary structures induced by NaCl, disturb the binding site and protein–RNA interaction.

Indeed, the secondary structure for 23S and 16S rRNA transcripts was altered in mutants lacking the two-envelope K^+/H^+ exchangers (Figure 7A). Furthermore, PAC protein immunoprecipitated from *kea1 kea2* bound less 23S rRNA than respective WT isolates, suggesting that access to its RNA-binding site may be sterically hindered or its affinity is reduced (Figure 7B). Disturbed ion homeostasis may also influence ribosomal assembly and function independently of rRNA processing. Optimal ribosomal function requires balanced concentrations of Mg^{2+}, K^+, and cationic polyamines in bacteria (Nierhaus, 2014). While it has been known for years that a lack or excess of K^+ prevents proper integrity and function of bacterial-type ribosomes (Bhaya and Jagendorf, 1984), research has focused primarily on mechanistically understanding the importance of Mg^{2+} for prokaryotic translation. Mg^{2+} ions play a key role in the stabilization of rRNA–protein interactions, ribosomal assembly, and tRNA-ribosome binding (Horlitz and Klaff, 2000; Blaha et al., 2002; Hirokawa et al., 2002; Konevega et al., 2004; Petrov et al., 2012). However, excess K^+ outcompetes Mg^{2+} for binding sites on ribosomal subunits, which impairs ribosome assembly and consequently protein synthesis (Nierhaus, 2014). A recent structural study in bacteria confirmed that K^+ ions play a direct role in stabilizing the ligand interactions between the translation machinery and messenger RNAs, transfer RNAs, ribosomal RNAs, and ribosomal proteins (Rozov et al., 2019). We cannot directly assign the phenotypic malfunction in *kea1 kea2* to stromal K^+ level due to the challenge of measuring the chloroplast ionome of the highly compromised mutants using standard elemental analytical techniques, such as ICP or total reflection X-ray fluorescence (TXRF). Employing a genetically encoded K^+ sensor targeted to the stroma may overcome the current technical barriers. Nevertheless, transport assays using reconstituted recombinant KEA2 protein, isolated WT versus *kea1 kea2* plastids, as well as complementation experiments with K^+ transport deficient yeast and *Escherichia coli* strains unanimously confirmed K^+/H^+ exchange for all KEA family members (Aranda-Sicilia et al., 2012; Zhu et al., 2018; Tsujii et al., 2019; Aranda Sicilia et al., 2021). Aranda-Sicilia demonstrated that stromal pH and thus likely K^+ level in isolated chloroplasts dynamically respond to light–dark transitions, which is in part dependent on KEA1/2 activity. Therefore, also a role of pH homeostasis and osmoregulation on the delayed development of mutant plastid should be considered. Interestingly, lack of KEA1/KEA2 barely altered the stromal steady-state pH in illuminated leaf plastids (Aranda Sicilia et al., 2021).

kea1 kea2 mutants exhibit increased K^+ content in green tissues, especially in developing young leaves (Höhner et al., 2016b, 2019). In line with previous research (Zhu et al., 1998; Stepien and Johnson, 2009; Chao et al., 2013), we have shown here that NaCl treatments and the concomitant competition between Na^+ and K^+ ions for uptake from the substrate result in K^+ depletion in WT but more strongly in mutant leaf cells (Table 1). This situation is favorable for *kea1 kea2* probably because less K^+ builds up in the mutant chloroplasts, partially resetting the stromal ion homeostasis. This explains the recovery of rRNA maturation, the increased steady-state plastome protein levels, and restored photosynthesis in salt-treated *kea1 kea2*. A similar rescue effect cannot be achieved if rRNA maturation is directly hampered, for instance through the loss of a cRBP as exemplified in *rap* and *rps5* mutants (Figure 5). Notably, treating *kea1 kea2* with equimolar KCl does not rescue but aggravates the mutant defects (Supplemental Figure S1). Therefore, it is reasonable to postulate the observed effects on plastid rRNA maturation and PGE in *kea1 kea2* mutants are primarily due to the failure to dynamically regulate stromal K^+ levels (and possibly pH). However, we cannot rule out the effect of other ion imbalances such as Mg^{2+}, which may be caused indirectly by the loss of KEA1/KEA2.

Lastly, we investigated which signaling pathways become activated to alter nuclear gene expression in response to plastid ion imbalance. Previous studies have shown that a lack of PGE triggers ROS production and the GUN1-dependent RS pathway (reviewed in Tadini et al., 2020; Colombo et al., 2016). Once activated, the RS pathway slows gene expression for nuclear-encoded chloroplast-targeted proteins by suppressing the TF GLK1 and downstream targets, the PhANGs, to protect the plant from additional photo-oxidative damage (Kakizaki et al., 2009; Leister and Kleine, 2016; Martin et al., 2016). Our results show that rRNA maturation defects in *kea1 kea2* hamper PGE, resulting in a strong suppression of *GLK1* and its downstream PhANG targets (Figure 10). Accordingly, we found that an additional loss of the key RS mediator GUN1 in *kea1 kea2* had dramatic consequences on plant vitality (Figure 11). In spite of this, surviving triple mutant individuals displayed significantly higher *GLK1* and PhANG transcript levels and increased chlorophyll content.

This research has revealed a previously uncharacterized *in vivo* effect of plastid ion transport on PGE, chloroplast-to-nucleus signaling, and nuclear gene expression resulting in dramatic changes in chloroplast development and delayed leaf greening. According to our model, the inner envelope K^+/H^+ exchangers *KEA1* and *KEA2* have an important role in setting up stromal ion and pH conditions for proper

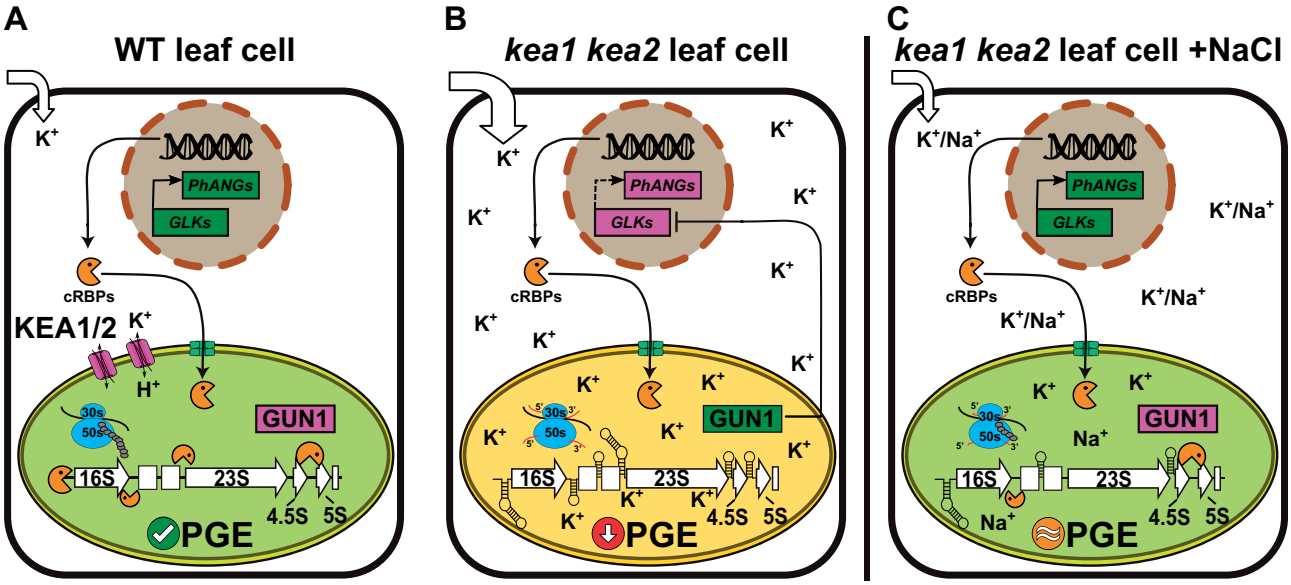

Figure 12 Model depicting the influence of chloroplast ion homeostasis on PGE in WT plants, and in the *kea1 kea2* mutant under control and NaCl treatment conditions. A, WT leaf cell under control conditions with functional KEA1/KEA2 transporters. In this cell, stromal buffer conditions are appropriate for rRNA processing, ribosome assembly, and ribosome activity, allowing for sufficient PGE. Thus, GUN1 remains inactive, and expression of the GLK1/GLK2 TFs and PhANGs establishes chloroplast development and photosynthesis. B, *kea1 kea2* leaf cell under control conditions. Disruption of ion transport increases cellular K^+, some of which accumulates in the plastid. This impairs plastome rRNA processing and ribosomal assembly/activity. The resulting disturbance of PGE triggers GUN1-mediated retrograde signaling to suppress the GLK1/GLK2 TFs and the expression of PhANGs. As a result, chloroplast biogenesis is delayed, and photosynthetic rates remain low. C, *kea1 kea2* leaf cell after treatment with NaCl. We predict salt treatment partially recovers stromal ion balance, by preventing K^+ accumulation in the cell and/or in the plastid. Thus, PGE is partially recovered. This keeps GUN1 signaling inactive, alleviating suppression of GLK1/GLK2 TFs and PhANG expression. The result is the execution of organelle biogenesis yielding photosynthesizing mutant chloroplasts.

plastid gene expression in WT leaf cells (Figure 12A). Simultaneous KEA1 and KEA2 loss-of-function perturbs leaf K^+ level and stromal buffer conditions, which affects RNA folding and RNA-protein interactions between cRBPs and their targets (Figure 12B). This results in a quantifiable chloroplast rRNA processing defect, decreased translation rates, and overall lower PGE. GUN1 senses PGE defects and other signs of plastid malfunction such as ROS. GUN1 initiates a signaling cascade that suppresses nuclear GLK1/GLK2 TFs. In the absence of GLK1/GLK2 TFs, PhANG expression remains low, thus halting chloroplast development, leaf greening, and photosynthesis (Waters et al., 2009). The addition of Na^+ partially restores leaf and stromal ion homeostasis to sufficiently recover rRNA maturation and PGE (Figure 12C). This keeps the GUN1-dependent RS pathway inactive and allows for increased expression of *GLK1* and PhANGs. The result is a timelier chloroplast development with improved photosynthetic rates in the *kea1 kea2* mutant under salt treatment.

In summary, our data show that the physiological significance of plastid ion transport goes beyond the well-known direct effects on photosynthesis. The activity of plastid ion transport proteins affects PGE, chloroplast biogenesis, and chloroplast-to-nucleus signaling. Each of these aspects also impacts photosynthetic rates. In other words, the primary role of KEA1/KEA2 is likely in plastid development and therefore many effects on photosynthetic activity are secondary. The results of this study have important implications for understanding stress physiology in crop plants and toward engineering photosynthesis. In recent years, changes to the plastid ion transportome have been pitched as a viable strategy to improve photosynthetic efficiency. However, this study shows that the organelle's ion transportome maintains a much wider set of functions within the biological system than previously understood, which need to be considered when pursuing this strategy.

Materials and methods

Germplasm and plant growth

Homozygous *kea1-1 kea2-1* (CS72318) and *kea1-2 kea2-2* (CS72319) were obtained from our previous study (Kunz et al., 2014). Except for *rps5-2*, all other loss-of-function lines were obtained from ABRC. Lines were confirmed to be homozygous using PCR with one gene-specific primer and one T-DNA-specific primer. For a full list of lines and primers, see Supplemental Table S4. Seeds were sterilized in 70% (v/v) ethanol, plated on ½ concentration Murashige and Skoog (MS) media with 0.8% (w/v) agar and stratified in the dark at 4°C for 48 h (Murashige and Skoog, 1962). Plates were then placed in growth chamber (CU-41L4; Percival Scientific) with 150 µmol photons $m^{-2}s^{-1}$ of continuous light (cool-white fluorescent bulbs), 16-h:8-h light: dark cycle. Growth temperatures were 22°C in the light and 18°C in the dark. Plants were grown for 7 days and then either

transferred to soil (Sungro Professional Growing Mix #1, Sun Gro Horticulture, USA) or to ½ MS agar plates with additional treatment. Plants transferred to soil were grown at the same light intensity, light cycle, and temperature described above in a Bio Chamber SPC-56 with florescent tubes (Phillips FS4T5/841HO) and LED bulbs (Satco LED A19 15.5 watt, 2700K). Treatment plates contained 67.5mM NaCl or respective NaCl or KCl amounts as given in the figure legend.

Elemental analysis

Leaf rosette elements from 3-week-old NaCl treated or untreated plants were analyzed via TXRF spectroscopy using an S4 T-STAR T-Star (Bruker) except for Na and Mg, which were analyzed by atomic absorption spectroscopy. All procedures were described in detail previously (Höhner et al., 2016b). Significant differences in the normalized mean were determined using an ordinary one-way analysis of variance (ANOVA) and Dunnett's multiple comparison test for parametric data, or a Kruskal–Wallis test and Dunn's multiple comparison test for nonparametric data ($P < 0.05$). All statistical analyses are available in Supplemental Dataset S6. Unless otherwise noted, all statistical tests were conducted using Graphpad Prism 8 (Graphpad Software Inc).

Chlorophyll fluorescence measurements

Chlorophyll fluorescence measurements were taken on 3-week-old plants as previously described (Kunz et al., 2009), unless otherwise stated. Plants were dark adapted for 20 min prior to imaging. Imaging was carried out on an Imaging PAM M-series chlorophyll fluorometer (Walz) using a built-in induction protocol for chlorophyll fluorescence kinetics with a photosynthetically active radiation intensity of 185 photons $m^{-2}s^{-1}$. Statistical evaluation was carried out for each figure containing PAM data as shown in Supplemental Dataset S6.

RNA isolation and sequencing

One-week-old Col-0 WT *A. thaliana* and independent *kea1 kea2* double-mutant lines were transferred to ½ MS agar media with or without 67.5 mM NaCl and grown for an additional 15 days (plants were 22 days old at harvest). For each treatment and genotype, there were three biological replicates. Total RNA was isolated from leaf tissue using the GeneJet Plant RNA purification kit (Thermo Fisher). Contaminating genomic DNA was removed via treatment with DNAse I (Thermo Fisher). Total RNA was then converted into a cDNA library using an Oligo(dT) polyA tail pulldown kit. Sequencing was carried out on an Illumina HiSeq 2500. Reads were 100 base pairs long, paired end, with over 15 million reads per sample. For details, see Supplemental Table S1. Raw sequencing data were reposited at the NCBI SRA public database (accession PRJNA573960, https://www.ncbi.nlm.nih.gov/sra/PRJNA573960).

RNA-SEQ data analysis

The raw fastq files were uploaded to the Illumina platform Basespace for further analysis through the Tuxedo Suite of RNA-SEQ analysis software. This pipeline includes the programs Bowtie, TopHat, Cufflinks, and Cuffdiff (Trapnell et al., 2012). These programs aligned raw reads to the TAIR10 *Arabidopsis* reference genome (Berardini et al., 2015), assembled transcripts, and subsequently called DEGs based on pairwise comparisons between each sample group. For this analysis, the FDR-adjusted *P* value (*q* value) was set to 0.05 to call significantly DEGs. For output files from Cuffdiff, see Supplemental Dataset S2. Subsequently, these genes were matched with a functional annotation from TAIR10 (Yon Rhee et al., 2003). The lists of DEGs from the WT versus mutant comparisons under both control and salt conditions were then further filtered for genes that were differentially expressed in both independent *kea1 kea2* mutant lines in the same direction to form a consensus DEG list. In other words, each gene on the consensus list was significantly up- or downregulated in both the WT comparison with *kea1-1kea2-1* and the comparison with *kea1-2 kea2-2*. Values from the consensus list for the control and salt treatment are labeled as "WC_KC" and "WS_KS," respectively, in the figures and text. For the full consensus DEG list in the control treatment comparison with corresponding values for the salt comparison, see Supplemental Dataset S3, sheet "WC_KC." For the full consensus DEG list in the salt comparison, see Supplemental Dataset S3, sheet "WS_KS." The consensus lists for both treatments from Supplemental Dataset S3 were first analyzed by the subcellular compartment localization prediction tool SUBA4 (Supplemental Figure S4; Hooper et al., 2017). The consensus lists for both treatments from Supplemental Dataset 3 were then used for functional enrichment analysis through the tool FUNC-E to find significantly enriched GO terms, PFAM protein families, and INTERPRO domains in *kea1 kea2* compared with WT under control and salt conditions (Ficklin and Alex Feltus, 2018). Annotations were pulled from the *DAVID* gene annotation tool website (Jiao et al., 2012). FUNC-E was run with a Fisher's *P* value cutoff of 0.01 (–ecut 0.01) and a high stringency (–preset high). Then, FDR-adjusted *P* values were calculated. FDR-adjusted *P* values for significantly enriched terms (FDR-adjusted $P < 0.01$) in the WC_KC comparison were mapped as heatmaps using Graphpad Prism 8 (Graphpad Software Inc). FDR-adjusted *P* values from the WS_KS comparison were mapped to the enriched terms from the WC_KC comparison, with nonsignificant annotations plotted in gray. For output files from FUNC-E, see Supplemental Dataset S4. Heatmaps of gene expression (Figure 3; Supplemental Figure S6) were created in Graphpad using $\log_2$ fold change values from comparisons with both independent *kea1 kea2* lines for significantly DEGs from the WC_KC consensus list (WC_KC1, WC_KC2, FDR-adjusted $P < 0.05$) and corresponding $\log_2$ fold changes for the salt treatment comparisons (WS_KS1, WS_KS2, nonsignificantly expressed genes plotted in gray). AGI numbers corresponding to gene names in heatmap are presented in

Supplemental Dataset S5. For the heatmaps of the GLK1/GLK2 signaling nexus (Figure 10), a list of downstream targets was curated from the genes shown to be most induced by GLK1/2 based on microarray data (Waters et al., 2009). Log_2 fold change values for statistically significantly DEGs from the WC_KC1, WC_KC2 and WS_KS1, and WS_KS2 comparisons (FDR-adjusted $P < 0.05$) in the list are plotted in color. Nonsignificant genes are gray. The heatmaps were then arranged in the vector graphics program Inkscape (open source).

Sodium Dodecyl Sulphate–Polyacrylamide Gel Electrophoresis (SDS–PAGE) and immunoblotting

To prepare samples, plants were grown on soil for 3 weeks as described above. About 20 mg of fresh weight from young or mature leaves was solubilized in 66 µL 4x Laemmli buffer; then, the final volume was adjusted to 200 µL with ddH_2O. Samples were incubated at 80°C for 10 min, and then spun at 6,000*g*. For each sample, 2.5 µL of supernatant (~ 0.25 mg FW) was loaded onto a 12% (w/v) polyacrylamide SDS–PAGE gel and run at 100V. Proteins were blotted from the gel onto 0.2-µm pore-size Biotrace NT nitrocellulose membrane (Pall Corporation) and blocked for 1 h in blocking buffer (Tween Tris buffered saline (TTBS) with 5% (w/v) nonfat milk powder). After rinsing three times for 5 min in TTBS, blots were incubated with 1:1,000 diluted respective primary antibody in TBS-T. RbcL (AS03037), RbcS (AS07259), V-ATPase (AS07213), PsbA (AS05084), and RPS5 (AS153075) antibodies were purchased (Agrisera). Custom antibodies included KEA1/KEA2 (Bölter et al., 2019), Tic40 (Stahl et al., 1999), Tic110 (Lübeck et al., 1996), LHCP (Clausen et al., 2004), PAC (Stoppel et al., 2011), and GLK1 (Tokumaru et al., 2017). Incubation was 1 h at room temperature, or overnight at 4°C. Subsequently, blots were rinsed in TTBS and incubated with secondary antibody (Peroxidase-conjugated Affinipure Goat Anti-Mouse Ig (H + L), Protein Tech) diluted 1:25,000 in blocking buffer for 90 min. Blots were then incubated with Clarity Western ECL Substrate (Bio-Rad) and imaged on a LICOR C-DiGit scanner (LICOR). For GLK1 detection, SuperSignal West Femto Maximum Sensitivity Substrate (Thermo Fisher) and ImageQuant LAS4000 (GE Healthcare) were used.

Array-based ribosome and transcript profiling of plastome-encoded genes

Ribosome footprints and total RNA were isolated as described in Zoschke et al. (2013), following the modifications introduced in (Trösch et al., 2018). RNA labeling and hybridization were performed according to Zoschke et al. (2013) with slight modifications: 3.5 µg purified footprints and 4 µg fragmented total RNA from *kea1 kea2* and WT (control and salt condition for each) were labeled with Cy3 and Cy5, respectively, using the ULS Small RNA Labelling Kit (Kreatech Diagnostics) according to the manufacturer's protocol. The analysis of ribosome profiling and transcriptome data was conducted as described in Trösch et al. (2018). Additional information in is provided in Supplemental Dataset S1.

RNA gel blot

About 300 ng total RNA was separated on 1.2% (w/v) agarose-formaldehyde gels as described previously (Beick et al., 2008). Separated RNAs were transferred to Hybond-N nylon membrane (GE Healthcare). The target transcripts were detected by hybridization at 50°C for the short (5′ and 3′) and at 65°C for the coding-region probes, respectively, with PCR products, which were body-labeled with [alpha-P32]-dCTP using random primers or sequence-specific reverse primers (see Supplemental Table S3). In order to prevent saturation effects for the detection of the highly abundant mature ribosomal RNA, 10 times cold probe (nonradioactive probe) was added to the hybridization reaction. The signals were detected by exposing phosphorimager screens to the radiolabeled membranes. Signals were quantified with Image Lab software (Bio-Rad).

DMS probing of RNA structure

Three-week-old plants were harvested and incubated in 1% of DMS freshly prepared in water for 4 min. Subsequently, DMS solution was replaced with ice-cold water and samples incubated on ice for 5 min. Leaves were frozen in liquid nitrogen and total RNA was extracted using TRIzol (Thermo Fisher Scientific) following the manufacturer's instructions. In total, 2 µg of total RNA was incubated in the presence of [gamma-32P]-ATP 5′-end-labeled primer (23S rRNA intern and 3′-end, 16S rRNA 3′-end, 4.5S rRNA and 5S rRNA 3′-end) and 0.5 mM dNTPs at 75°C for 5 min. Subsequently, the temperature was dropped to 50°C, SSIV RT enzyme mix (Thermo Fisher Scientific) added according to the manufacturer's protocol for first-strand cDNA synthesis reaction and incubated for 30 min. The reaction was stopped by adding one volume of RNA loading buffer (90% deionized formamide, 20 mM Tris pH 8.0, 20 mM EDTA, traces of bromophenol blue, and xylene cyanole) and by incubating at 95°C for 5 min. Extension products were loaded onto an 8% polyacrylamide gel containing 8 M urea and run in 1×Tris-Borate-EDTA (TBE) buffer.

RNA-Co-IP

About 200 mg of ground tissue from 3-week-old plants was resuspended in 200 µL Co-IP buffer (100 mM Tris pH 8.0, 150 mM NaCl, 5 mM EDTA, 5 mM EGTA, 0.5% Triton X-100, cOmplete EDTA-free Protease Inhibitor Cocktail [Roche], and 40 U of RNase Inhibitor [Thermo Fisher Scientific]) and incubated on ice for 20 min. Following 15-min centrifugation 20,000*g* at 4°C, the supernatant (1 mg) was incubated under gentle rotation with PAC-specific antibodies or control IgGs for 1 h at 4°C. IgGs were captured with SureBeads Protein A Mag beads (Bio-Rad). Co-precipitated RNA was recovered by TRIzol extraction followed by phenol/chloroform/isoamyl-alcohol extraction and ethanol precipitation. Half of the pellet RNA and $1/80^{th}$ of the supernatants were heated at 70°C for 10 min in 2x SSPE

buffer (300 mM NaCl, 20 mM NaH_2PO_4, and 2 mM EDTA pH 7.4) and blotted onto Hybond-N+ membrane (GE Healthcare) using a slot blot system (GE Healthcare). Membranes were hybridized with 16S and 23S rRNA-specific 80-mers as described in polysome loading section. To check for successful immunoprecipitation ca. 50 µg of the input and supernatant along with 1/10th of each IP fraction was separated via SDS PAGE, blotted onto a PVDF membrane and incubated with PAC-specific antibodies (1:3,000).

Polysome loading

Polysome loading experiment was performed as described previously (Meurer et al., 2017). [γ-^{32}P]ATP 5′-end-labeled 80-mers were used as probes. Hybridization was performed with PerfectHybTM Plus Hybridization Buffer (Sigma) at 55°C for 3 h. Membranes were washed twice at 55°C for 5 min with buffer containing 1× SSC and 0.1% SDS.

RT-qPCR

Total RNA was extracted and treated with DNase I as described for the RNA-SEQ experiment. After removal of genomic DNA, a cDNA pools were prepared using a Revertaid FirstStrand cDNA synthesis kit with Oligo(dT)$_{18}$ primers (Thermo Fisher). RT-qPCR reactions were run using PerfeCta SYBR Green FastMix (QuantaBio), with 15 ng of template cDNA, and 300 nM final concentration of each primer per reaction. For lists of primers, see Supplemental Table S5. Three biological replicates of each sample and two technical replicates of each biological replicate were run in a Biorad CFX96 Real-Time thermocycler. PCR parameters can be found in Supplemental Table S6. This experiment was run independently three times, and a ΔC_q value was calculated for each reaction using *SAND* or *TIP2* as a house-keeping gene, as both genes show low variation in expression under different light conditions (Czechowski et al., 2005). Technical replicates for each biological replicate were averaged, and each biological replicate was normalized to the average WT level of expression. These normalized values were then used to calculate the mean and standard error of the mean (SEM) for each genotype. Significant differences in the normalized mean were determined using an ordinary one-way ANOVA and Tukey's multiple Comparison test for parametric data, or a Kruskal–Wallis test and Dunn's multiple comparisons test for nonparametric data ($P < 0.05$).

Chlorophyll determination

About 20 mg of leaf tissue from 24-day-old plants was ground in liquid nitrogen, and then incubated in 80% (v/v) acetone for 1 h on ice in the dark, vortexing occasionally. Samples were then spun at maximum speed for 5 min at 4°C. The absorbance of the supernatant at 646, 663, and 750 nm was measured in a spectrophotometer. The chlorophyll content was calculated from the absorption at these wavelengths as described previously (Porra et al., 1989). Statistically significant differences in mean chlorophyll content between genotypes were determined by use of a Kruskal–Wallis test and Dunn's multiple comparisons test for nonparametric data ($P < 0.05$).

Hypocotyl elongation assays

WT, *kea1-1kea2-1*, *kea1-2 kea2-2*, *phyA-211* (Nagatani et al., 1993), and *phyB-9* (Reed et al., 1993) seeds were sterilized as described in the plant growth section, but then plated in 25 mm-deep petri dishes. Seeds were stratified for 2–3 days at 4°C. Plates were then placed in 50 µmol photons $m^{-2}s^{-1}$ of light of red light (RL, $\lambda = 627$ nm, 14–16-h light: 8–10-h dark) in a Fytoscope (Photon Systems Instruments) for 12 h to stimulate germination. After 12 h, the plates were either transferred to 5 µmol photons m^{-2} s^{-1} of constant far-red light (FRL, $\lambda = \sim 750$ nm) or remained in RL as described above for 4 more days. Hypocotyl lengths were measured by removing seedlings from agar, photographing flat, then quantifying hypocotyl length using the Simple Nuerite Tracer in Fiji image analysis software. Hypocotyl lengths were then normalized to the mean of the dark control of each genotype, and significant differences in the normalized mean were determined using a Kruskal–Wallis test and Dunn's multiple comparisons test ($P < 0.05$).

ROS staining

H_2O_2 staining was carried out by incubating rosettes in 3,3′-diaminobenzidine (DAB), which forms a brown precipitate when reduced by H_2O_2 (Arsalan Daudi, 2012). Rosettes from control and salt-treated WT, *kea1-1kea2-1*, and *kea1-2 kea2-2* were vacuum infiltrated with 1% (w/v) DAB as previously described (Arsalan Daudi, 2012). Infiltrated rosettes were exposed to 200 µmol photons $m^{-2}s^{-1}$ of white light for 8 h to induce H_2O_2 production. As a negative control, some DAB infiltrated rosettes were incubated in the dark. Chlorophyll was bleached from the plants by boiling in a 3:1:1 solution of ethanol, acetic acid, and glycerol for 15 min. The % leaf area stained with DAB was quantified in Fiji image analysis software. Significant differences in the normalized mean were determined using a using a Kruskal–Wallis test and Dunn's multiple comparisons test ($P < 0.05$).

Pulse-chase labeling of leaves

About 5 mg of tissue was punched from young and mature leaves of each genotype and placed into microfuge tubes. Punches were vacuum infiltrated with 50 µL of reaction buffer (1 mM KH_2PO_4 pH 6.3, 75 µM cycloheximide) and incubated on ice in the dark for 30 min. Tissue was then infiltrated with 10 µCi of Express ^{35}S Protein Labelling Mix (Perkin Elmer) and incubated at 25°C under 300 photons $m^{-2}s^{-1}$ of white light. For the chase, samples were washed once with incubation buffer, then once with chase buffer (reaction buffer with 10 mM L-cysteine, 10 mM L-methionine). Samples were then vacuum infiltrated with 50 µL of chase buffer and placed back under light. Samples were processed at each timepoint by washing twice in 200 mM Na_2CO_3, then homogenized in 50 µL of 100 mM Na_2CO_3, mixed with 33 µL 4× Laemmli buffer, and incubated at 80°C for 10 min. Samples where then spun at 1,000*g* for 5

min. Supernatant was loaded onto a 12% (w/v) polyacrylamide SDS–PAGE gel and run at 100 V for 1–2 h. Gels were then Coomassie stained, dried, and applied to a phosphor screen for 12–16 h. Screen was imaged on a Typhoon Phosphorimager (GE Lifesciences). The intensity of the radioactive label in different bands on the gel was quantified in ImageJ. To quantify total labelled protein, lanes of the gel were run through a scintillation counter. Values were normalized to fresh weight, and then to the WT control for each experiment. Mean rates of protein accumulation were determined to be different from the WT control using a Šídák's multiple comparisons test ($P < 0.05$).

Spectinomycin susceptibility assay

Plates for spectinomycin plates were prepared as described in the plant growth section except that sterilized seeds were directly sown on treatment media. Spectinomycin treatment plates contained 0, 1, 3, 5, and 7 μg ml^{-1} spectinomycin dihydrochloride. Plants were then grown for 14 days in the light and temperature conditions described in the plant growth section. Survival rates were calculated by dividing the number of plants with developed true leaves by the total number of germinated seedlings for each genotype. The *rap-1* genotype was predisposed toward poor growth. Thus, the survival rate for each genotype was normalized to the 0 μg ml^{-1} spectinomycin treatment. Significant differences in survival rates from the WT at each spectinomycin concentration were determined using a Kruskal–Wallis test and Dunn's Multiple Comparisons test ($P < 0.05$).

In vitro protein translation

Reading frames for FNR and PDHe1α (At1g01090) were cloned into pGEM®-5Zf(+) Vector. *In vitro* translation of protein import substrates was performed applying the SP6 TNT coupled transcription/translation kit (Promega, WI, USA) in the presence of ^{35}S labeled Met/Cys for 60 min at 30°C.

Chloroplast isolation and import

Seeds from respective lines were surface sterilized and sown on ½ MS with 1% (w/v) sucrose plates. After 3 weeks at 21°C, 16-h light: 8-h dark, plants were harvested using a razor blade from one (WT) or two (*kea1-1kea2-1*, *kea1-2 kea2-2*) plates, respectively. Leaf material was homogenized with a polytron mixer for 1–2 s in 25 mL of isolation buffer (0.3 M sorbitol, 5 mM $MgCl_2$, 5 mM EDTA, 20 mM HEPES, 10 mM $NaHCO_3$, pH 8.0 with KOH). Homogenate was then filtered through four layers of cheesecloth and 1 layer of Miracloth. Filtrate was centrifuged for 4 min at 1,500*g* and 4°C. Supernatant was discarded, and pellet was gently resuspended in 1 mL of isolation buffer and layered over a Percoll step gradient (30%, 82% Percoll in 0.3 M sorbitol 5 mM $MgCl_2$, 5 mM EDTA, 20 mM HEPES–NaOH pH 8.0) and centrifuged at 2,000*g* for 6 min. The lower band containing intact chloroplasts was carefully removed. Intact chloroplasts were mixed in three volumes of wash buffer (50 mM HEPES, 0.3 M sorbitol, 3 mM $MgSO_4$, pH 8.0 with KOH) and centrifuged for 4 min at 1,500*g* and 4°C. The final pellets were resuspended in a small volume of wash buffer, and chlorophyll concentration was determined according as previously described (Arnon, 1949). Import was conducted in wash buffer containing 3 mM Na-ATP, 10 mM L-Met, 10 mM L-Cys, 50 mM ascorbic acid, 20 mM K-gluconate, 10 mM $NaHCO_3$, 0.2% (w/v) BSA plus 2-μL translation product for 8 min at 25°C. Afterward, chloroplasts were pelleted at 1,500*g*, washed once in 200 μL wash buffer, and then resuspended in SDS loading buffer. Proteins were separated on SDS gels, which were Coomassie stained, and then vacuum dried and exposed on a Phosphorimager Screen for 14 h. Screens were analyzed by a Typhoon Phosphorimager (GE Healthcare) and radioactive bands were quantified with Image Quant (GE Healthcare). In general, WT chloroplasts equivalent to 10–15 μg chlorophyll were used per import. Since *kea1 kea2* mutants have reduced chlorophyll content, equal plastid amounts per assay were quantified based on Coomassie-stained bands from the SDS–PAGE using Image Quant (GE Healthcare). Bands corresponding to RbcL and the LHC proteins were excluded from the quantification since *kea1 kea2* has a preexisting deficiency in these typically high abundance proteins. For statistical evaluation, the amount of WT chloroplasts was set to 100%, as was the imported protein. All experiments were performed from three different chloroplast isolations.

Statistical analysis

For specifics on statistical tests related to RNA-SEQ, see "RNA Sequencing (RNA-SEQ) Data Analysis" in "Methods". All statistical tests not related to the RNA-SEQ analysis were conducted in GraphPad Prism™ version 8. Universally, error bars represent ±SEM, and $\alpha = 0.05$ ($P < 0.05$). For comparison of means influenced by two independent variables, a two-way ANOVA was used in conjunction with Tukey's multiple comparisons test or or Šídák's multiple comparisons test depending on the types of comparisons made. For comparisons of means of normally distributed data influenced by one independent variable, an ordinary one-way ANOVA was used in conjunction with either Tukey's multiple comparisons test or Dunnett's multiple comparisons test depending on the types of comparisons made. For comparisons of means of nonparametric data influenced by one independent variable, a Kruskal–Wallis test with Dunn's multiple comparisons test was used. Details about the specific test used for each figure, table, and supplemental figure are provided in Supplemental Dataset S6.

Accession numbers

These genetic loci were important to this project: KEA1 (AT1G01790), KEA2 (AT4G00630), GLK1 (AT2G20570), GLK2 (AT5G44190), GUN1 (AT2G31400), VAR2 (AT2G30950), RAP (AT2G31890), RPS5 (AT2G33800), PAC (AT2G48120), PHYA (AT1G09570), PHYB (AT2G18790), LHCB1.2 (AT1G29910), LHCB2.2 (AT2G05070), SAND (AT2G28390), and TIP2 (AT3G26520). For information on T-DNA insertion lines, see Supplemental Table S4. For

information about use of these loci for RT-qPCR, see Supplemental Table S5.

Supplemental data

The following materials are available in the online version of this article.

Supplemental Figure S1. KCl treatment exacerbates the *kea1 kea2* photosynthetic phenotype, while NaCl rescues phenotype.

Supplemental Figure S2. Principal component analysis.

Supplemental Figure S3. Volcano Plots of RNA Sequencing Comparisons.

Supplemental Figure S4. SUBA4 Multiple Marker Abundance Profiling (MMAP) tool applied to lists of DEGs reveals many differentially expressed transcripts in *kea1 kea2* encode chloroplast-targeted proteins.

Supplemental Figure S5. Venn Diagram of Overlapping DEGs for control and NaCl comparisons.

Supplemental Figure S6. Log_2 fold change expression of genes with annotations of interest.

Supplemental Figure S7. Chloroplast protein import rates are similar in *kea1 kea2* and WT, indicating that import of RNA-binding proteins is not impaired.

Supplemental Figure S8. Replicate immunoblots.

Supplemental Figure S9. Autoradiographs from the pulse-chase analyses.

Supplemental Figure S10. Hypocotyl Elongation under monochromatic light for WT, *kea1 kea2*, and *phya* or *phyb* controls.

Supplemental Figure S11. DAB stain for H_2O_2 production shows *kea1 kea2* accumulates more ROS than the WT under control conditions, but not under NaCl treatment.

Supplemental Figure S12. Chlorophyll A, Chlorophyll B, and Chlorophyll A/B ratios in *gun1*, *kea1 kea2*, and triple mutants.

Supplemental Table S1. RNA sequencing statistics.

Supplemental Table S2. Differentially expressed genes.

Supplemental Table S3. RNA blot primers.

Supplemental Table S4. Genotypes used in this study.

Supplemental Table S5. RT-qPCR primers.

Supplemental Table S6. RT-qPCR thermocycle protocol.

Supplemental Dataset S1. Complete dataset from transcript and ribosome profiling analyses of *kea1 kea2* and WT under control and salt stress conditions.

Supplemental Dataset S2. Output files from Cuffdiff.

Supplemental Dataset S3. Consensus list of DEGs for WT versus *kea1 kea2* control comparison, and salt treatment comparison.

Supplemental Dataset S4. Output from FUNC-E analysis.

Supplemental Dataset S5. AGI number and Log_2 fold change for genes presented in heatmaps.

Supplemental Dataset S6. Statistics information.

Acknowledgments

We thank Dr Jürgen Soll (Ludwig Maximilian University) for providing antibodies and training in protein work. Dr Li Li (Cornell University) kindly provided *rps5-2* germplasm. We thank Drs Michael Neff and Helmut Kirchhoff (Washington State University, WSU) for providing *phya* and *phyb* loss-of-function lines and access to monochromatic light chambers, respectively. Thanks to Drs Samaneh Tabatabaei and Ursula Fittschen (WSU) for training, assistance, and equipment access to analyze leaf elements. Dr. Kiwamu Tanaka and Matt Marcec (WSU) gave guidance on RT-qPCR and equipment access. We thank WSU scientists Drs. Stephen Ficklin and Dorrie Main for advice and training on RNA-SEQ analysis and Drs Omar Cornejo and Allison Kolbe for early discussion on transcriptomics. We are grateful for technical undergrad assistance by WSU alumni: Eben Diederich and Simon Alsager. Finally, we thank Dr John Browse and his lab (WSU) for providing access to facilities for radioactive isotope labeling and imaging. Working within a community of generous and supportive scientists has been a pleasure.

Funding

H.-H.K. and R.A.D. were funded by an National Science Foundation (NSF) Career Award IOS-1553506 to H.-H.K. Elemental analysis was realized through an NSF MRI-1828266 award to H.-H.K. R.A.D. was supported by NIH Biotechnology Training Program, ARCS Foundation Fellowship, and the NSF Graduate Research Fellowship Program. B.B. and S.S. received funding from the Deutsche Forschungsgemeinschaft (DFG) (SFB-TR 175, project B06). R.Z. was funded by DFG (SFB-TR 175, project A04; ZO 302/5-1). N.M. and J.M. were funded by DFG (SFB-TR 175, project A03). T.I. was supported by a Grant-in-Aid for Scientific Research (18H02169) from Japan Society for the Promotion of Science (JSPS).

Conflict of interest statement. None declared.

References

Adhikari ND, Froehlich JE, Strand DD, Buck SM, Kramer DM, Larkin RM (2011) GUN4-porphyrin complexes bind the ChlH/GUN5 subunit of Mg-chelatase and promote chlorophyll biosynthesis in *Arabidopsis*. Plant Cell **23**: 1449–1467

Allen JF, de Paula WBM, Puthiyaveetil S, Nield J (2011) A structural phylogenetic map for chloroplast photosynthesis. Trends Plant Sci **16**: 645–655

Aranda-Sicilia MN, Cagnac O, Chanroj S, Sze H, Rodríguez-Rosales MP, Venema, K (2012) Arabidopsis KEA2, a homolog of bacterial KefC, encodes a K^+/H^+ antiporter with a chloroplast transit peptide. Biochim Biophys Acta **1818**: 2362–2371

Aranda-Sicilia MN, Aboukila A, Armbruster U, Cagnac O, Schumann T, Kunz HH, Jahns P, Rodriguez-Rosales MP, Sze H, Venema K (2016) Envelope K^+/H^+ antiporters AtKEA1 and AtKEA2 function in plastid development. Plant Physiol **172**: 441–449

Aranda Sicilia MN, Sánchez Romero ME, Rodríguez Rosales MP, Venema K (2021) Plastidial transporters KEA1 and KEA2 at the inner envelope membrane adjust stromal pH in the dark. New Phytol **229**: 2080–2090

Arnon DI (1949) Copper enzymes in isolated chloroplasts. Polyphenoloxidase in Beta Vulgaris. Plant Physiol **24**: 1

Arsalan Daudi JOB (2012) Detection of hydrogen peroxide by DAB staining in Arabidopsis leaves. Bio protoc **2**: e263.

Barkan A (2011) Expression of plastid genes: organelle-specific elaborations on a prokaryotic scaffold. Plant Physiol **155**: 1520

Barkan A, Small I (2014) Pentatricopeptide repeat proteins in plants. *In* SS Merchant, ed, Annual Review of Plant Biology, Vol. **65**. Annual Reviews, Palo Alto, p 415

Beick S, Schmitz-Linneweber C, Williams-Carrier R, Jensen B, Barkan A (2008) The pentatricopeptide repeat protein PPR5 stabilizes a specific tRNA precursor in maize chloroplasts. Mol Cell Biol **28**: 5337

Berardini TZ, Reiser L, Li D, Mezheritsky Y, Muller R, Strait E, Huala E (2015) The arabidopsis information resource: making and mining the "gold standard" annotated reference plant genome. Genesis **53**: 474–485

Berry JO, Yerramsetty P, Zielinski AM, Mure CM (2013) Photosynthetic gene expression in higher plants. Photosynth Res **117**: 91–120

Bhaya D, Jagendorf AT (1984) Optimal conditions for translation by thylakoid-bound polysomes from pea chloroplasts. Plant Physiol **75**: 832–838

Blaha G, Burkhardt N, Nierhaus KH (2002) Formation of 70S ribosomes: large activation energy is required for the adaptation of exclusively the small ribosomal subunit. Biophys Chem **96**: 153–161

Bollenbach TJ, Lange H, Gutierrez R, Erhardt M, Stern DB, Gagliardi D (2005) RNR1, a 3'-5' exoribonuclease belonging to the RNR superfamily, catalyzes 3' maturation of chloroplast ribosomal RNAs in *Arabidopsis thaliana*. Nucleic Acids Res **33**: 2751–2763

Bölter B, Mitterreiter MJ, Schwenkert S, Finkemeier I, Kunz HH (2019) The topology of plastid inner envelope potassium cation efflux antiporter KEA1 provides new insights into its regulatory features. Photosynth Res **145**: 43–54.

Börner T, Aleynikova AY, Zubo YO, Kusnetsov VV (2015) Chloroplast RNA polymerases: role in chloroplast biogenesis. Biochim Biophys Acta, Bioenerg **1847**: 761–769

Brink MF, Brink G, Verbeet MP, de Boer HA (1994) Spectinomycin interacts specifically with the residues G1064 and C1192 in 16S rRNA, thereby potentially freezing this molecule into an inactive conformation. Nucleic Acids Res **22**: 325–331

Chanroj S, Wang G, Venema K, Zhang MW, Delwiche CF, Sze H (2012) Conserved and diversified gene families of monovalent cation/H+ antiporters from algae to flowering plants. Front Plant Sci **3**: 25

Chao DY, Dilkes B, Luo HB, Douglas A, Yakubova E, Lahner B, Salt DE (2013) Polyploids exhibit higher potassium uptake and salinity tolerance in *Arabidopsis*. Science **341**: 658–659

Cheng JA, He CX, Zhang ZW, Xu F, Zhang DW, Wang X, Yuan S, Lin HH (2011) Plastid signals confer Arabidopsis tolerance to water stress. Z Naturforsch(C) **66**: 47–54

Colombo M, Tadini L, Peracchio C, Ferrari R, Pesaresi P (2016) GUN1, a jack-of-all-trades in chloroplast protein homeostasis and signaling. Front Plant Sci **7**

Clausen C, Ilkavets I, Thomson R, Philippar K, Vojta A, Möhlmann T, Neuhaus E, Fulgosi H, Soll J (2004) Intracellular localization of VDAC proteins in plants. Planta **220**: 30–37

Czechowski T, Stitt M, Altmann T, Udvardi MK, Scheible W-R (2005) Genome-wide identification and testing of superior reference genes for transcript normalization in Arabidopsis. Plant Physiol **139**: 5–17

D'Alessandro S, Ksas B, Havaux M (2018) Decoding β-cyclocitral-mediated retrograde signaling reveals the role of a detoxification response in plant tolerance to photooxidative stress. Plant Cell **30**: 2495

de Vries J, Archibald JM (2018) Plastid autonomy vs nuclear control over plastid function. *In* SM Chaw, RK Jansen, eds, Plastid Genome Evolution. Academic Press Ltd-Elsevier Science Ltd, London, pp 1–28.

Draper DE, Grilley D, Soto AM (2005) Ions and RNA folding. Annu Rev Biophys Biomol Struct **34**: 221–243

Estévez JM, Cantero A, Reindl A, Reichler S, León P (2001) 1-Deoxy-d-xylulose-5-phosphate synthase, a limiting enzyme for plastidic isoprenoid biosynthesis in plants. J Biol Chem **276**: 22901–22909

Ficklin S, Alex Feltus F (2018, May 14) SystemsGenetics/FUNC-E v1.0 (Version v1.0). Zenodo. 10.5281/zenodo.1246882

Finazzi G, Petroutsos D, Tomizioli M, Flori S, Sautron E, Villanova V, Rolland N, Seigneurin-Berny D (2015) Ions channels/transporters and chloroplast regulation. Cell Calcium **58**:86–97 10.1016/j.ceca.2014.10.002

Fitter DW, Martin DJ, Copley MJ, Scotland RW, Langdale JA (2002) GLK gene pairs regulate chloroplast development in diverse plant species. Plant J **31**: 713–727

Fukazawa H, Tada A, Richardson LGL, Kakizaki T, Uehara S, Ito-Inaba Y, Inaba T (2020) Induction of TOC and TIC genes during photomorphogenesis is mediated primarily by cryptochrome 1 in Arabidopsis. Sci Rep **10**: 20255

Gawroński P, Pałac A, Scharff LB (2020) Secondary structure of chloroplast mRNAs in vivo and in vitro. Plants **9**

Hammani K, Bonnard G, Bouchoucha A, Gobert A, Pinker F, Salinas T, Giege P (2014) Helical repeats modular proteins are major players for organelle gene expression. Biochimie **100**: 141–150.

Hernandez-Verdeja T, Strand A (2018) Retrograde signals navigate the path to chloroplast development. Plant Physiol **176**: 967–976.

Hirokawa G, Kiel MC, Muto A, Kawai G, Igarashi K, Kaji H, Kaji A (2002) Binding of ribosome recycling factor to ribosomes, comparison with tRNA. J Biol Chem **277**: 35847–35852

Höhner R, Aboukila A, Kunz H-H, Venema K (2016a) Proton gradients and proton-dependent transport processes in the chloroplast. Front Plant Sci **7**: 218

Höhner R, Tabatabaei S, Kunz H-H, Fittschen U (2016b) A rapid total reflection X-ray fluorescence protocol for micro analyses of ion profiles in *Arabidopsis thaliana*. Spectrochim Acta Part B **125**: 159–167

Höhner R, Galvis VC, Strand DD, Völkner C, Krämer M, Messer M, Dinc F, Sjuts I, Bölter B, Kramer DM, et al. (2019). Photosynthesis in Arabidopsis is unaffected by the function of the vacuolar K^+ channel TPK3. Plant Physiol **180**: 1322

Hooper CM, Castleden IR, Tanz SK, Aryamanesh N, Millar AH (2017) SUBA4: the interactive data analysis centre for Arabidopsis subcellular protein locations. Nucleic Acids Res **45**: D1064–D1074

Horlitz M, Klaff P (2000) Gene-specific trans-regulatory functions of magnesium for chloroplast mRNA stability in higher plants. J Biol Chem **275**: 35638–35645

Jarvis P, Soll J (2001) Toc, Tic, and chloroplast protein import. Biochim Biophys Acta (BBA) Mol Cell Res **1541**: 64–79

Jiao X, Sherman BT, Huang DW, Stephens R, Baseler MW, Lane HC, Lempicki RA (2012) DAVID-WS: a stateful web service to facilitate gene/protein list analysis. Bioinformatics (Oxford, England) **28**: 1805–1806

Kacprzak SM, Mochizuki N, Naranjo B, Xu DR, Leister D, Kleine T, Okamoto H, Terry MJ (2019). Plastid-to-nucleus retrograde signalling during chloroplast biogenesis does not require ABI4. Plant Physiol **179**: 18–23

Kakizaki T, Matsumura H, Nakayama K, Che F-S, Terauchi R, Inaba T (2009) Coordination of plastid protein import and nuclear gene expression by plastid-to-nucleus retrograde signaling. Plant Physiol **151**: 1339

Kleine T, Leister D (2016) Retrograde signaling: organelles go networking. Biochim Biophys Acta Bioenerg **1857**: 1313–1325

Kleinknecht L, Wang F, Stübe R, Philippar K, Nickelsen J, Bohne A-V (2014) RAP, the sole octotricopeptide repeat protein in Arabidopsis, is required for chloroplast 16S rRNA maturation. Plant Cell **26**: 777–787

Köhler D, Helm S, Agne B, Baginsky S (2016) Importance of translocon subunit Tic56 for rRNA processing and chloroplast ribosome assembly. Plant Physiol **172**: 2429

Konevega AL, Soboleva NG, Makhno VI, Semenkov YP, Wintermeyer W, Rodnina MV, Katunin VI (2004) Purine bases at position 37 of tRNA stabilize codon-anticodon interaction in the ribosomal A site by stacking and Mg^{2+}-dependent interactions. RNA (New York, N.Y.) **10**: 90–101.

Kunz H-H, Scharnewski M, Feussner K, Feussner I, Flügge U-I, Fulda M, Gierth M (2009) The ABC transporter PXA1 and peroxisomal β-oxidation are vital for metabolism in mature leaves of Arabidopsis during extended darkness. Plant Cell **21**: 2733–2749

Kunz HH, Gierth M, Herdean A, Satoh-Cruz M, Kramer DM, Spetea C, Schroeder JI (2014) Plastidial transporters KEA1, -2, and -3 are essential for chloroplast osmoregulation, integrity, and pH regulation in Arabidopsis. Proc Natl Acad Sci U S A **111**: 7480–7485

Leister D, Kleine T (2016) Definition of a core module for the nuclear retrograde response to altered organellar gene expression identifies GLK overexpressors as gun mutants. Physiol Plant **157**: 297–309.

Leister D, Wang LS, Kleine T (2017). Organellar gene expression and acclimation of plants to environmental stress. Front Plant Sci **8**: 10

Lübeck J, Soll J, Akita M, Nielsen E, Keegstra K (1996) Topology of IEP110, a component of the chloroplastic protein import machinery present in the inner envelope membrane. EMBO J **15**: 4230–4238

Manavski N, Schmid L-M, Meurer J (2018) RNA-stabilization factors in chloroplasts of vascular plants. Essays Biochem **62**: 51–64

Mandel MA, Feldmann KA, Herrera-Estrella L, Rocha-Sosa M, León P (1996) CLA1, a novel gene required for chloroplast development, is highly conserved in evolution. Plant J **9**: 649–658

Martin G, Leivar P, Ludevid D, Tepperman JM, Quail PH, Monte E (2016) Phytochrome and retrograde signalling pathways converge to antagonistically regulate a light-induced transcriptional network. Nat Commun **7**: 10

McCormac AC, Fischer A, Kumar AM, Söll D, Terry MJ (2001) Regulation of HEMA1 expression by phytochrome and a plastid signal during de-etiolation in *Arabidopsis thaliana*. Plant J **25**: 549–561

McDermott JJ, Civic B, Barkan A (2018) Effects of RNA structure and salt concentration on the affinity and kinetics of interactions between pentatricopeptide repeat proteins and their RNA ligands. PLOS ONE **13**: e0209713

Meurer J, Schmid L-M, Stoppel R, Leister D, Brachmann A, Manavski N (2017) PALE CRESS binds to plastid RNAs and facilitates the biogenesis of the 50S ribosomal subunit. Plant J **92**: 400–413

Murashige T, Skoog F (1962) A revised medium for rapid growth and bio assays with tobacco tissue cultures. Physiol Plant **15**: 473–497

Nagatani A, Reed JW, Chory J (1993) Isolation and initial characterization of Arabidopsis mutants that are deficient in phytochrome A. Plant Physiol **102**: 269

Neff MM, Chory J (1998) Genetic interactions between phytochrome A, phytochrome B, and cryptochrome 1 during Arabidopsis development. Plant Physiol **118**: 27

Nierhaus KH (2014) Mg^{2+}, K^{+}, and the ribosome. J Bacteriol **196**: 3817–3819

Oh S, Montgomery BL (2014) Phytochrome-dependent coordinate control of distinct aspects of nuclear and plastid gene expression during anterograde signaling and photornorphogenesis. Front Plant Sci **5**: 8

Paddock T, Lima D, Mason ME, Apel K, Armstrong GA (2012) Arabidopsis light-dependent protochlorophyllide oxidoreductase A (PORA) is essential for normal plant growth and development. Plant Mol Biol **78**: 447–460

Petrov AS, Bernier CR, Hsiao CL, Okafor CD, Tannenbaum E, Stern J, Gaucher E, Schneider D, Hud NV, Harvey SC, et al. (2012). RNA-magnesium-protein interactions in large ribosomal subunit. J Phys Chem B **116**: 8113–8120

Pittman J (2012) Multiple transport pathways for mediating intracellular pH homeostasis: the contribution of H+/ion exchangers. Front Plant Sci **3**:11

Pogson BJ, Albrecht V (2011) Genetic dissection of chloroplast biogenesis and development: an overview. Plant Physiol **155**: 1545–1551

Porra RJ, Thompson WA, Kriedemann PE (1989) Determination of accurate extinction coefficients and simultaneous-equations for assaying chlorophyll-a and chlorophyll-b extracted with 4 different solvents - verification of the concentration of chlorophyll standards by atomic-absorption spectroscopy. Biochim Biophys Acta **975**: 384–394

Reed JW, Nagpal P, Poole DS, Furuya M, Chory J (1993) Mutations in the gene for the red far-red light receptor phytochrome-b alter cell elongation and physiological-responses throughout Arabidopsis development. Plant Cell **5**: 147–157

Rozov A, Khusainov I, El Omari K, Duman R, Mykhaylyk V, Yusupov M, Westhof E, Wagner A, Yusupova G (2019) Importance of potassium ions for ribosome structure and function revealed by long-wavelength X-ray diffraction. Nat Commun **10**: 12

Ruckle ME, DeMarco SM, Larkin RM (2007) Plastid signals remodel light signaling networks and are essential for efficient chloroplast biogenesis in Arabidopsis. Plant Cell **19**: 3944–3960

Schmitz-Linneweber C, Small I (2008) Pentatricopeptide repeat proteins: a socket set for organelle gene expression. Trends Plant Sci **13**: 663–670

Schroppelmeier G, Kaiser WM (1988) Ion homeostasis in chloroplasts under salinity and mineral deficiency: I. Solute concentrations in leaves and chloroplasts from spinach plants under NaCl or $NaNO_3$ salinity. Plant Physiol **87**: 822–827

Stahl T, Glockmann C, Soll J, Heins L (1999) Tic40, a New "Old" Subunit of the Chloroplast Protein Import Translocon. J Biol Chem **274**: 37467–37472

Stepien P, Johnson GN (2009) Contrasting responses of photosynthesis to salt stress in the glycophyte Arabidopsis and the halophyte thellungiella: role of the plastid terminal oxidase as an alternative electron sink. Plant Physiol **149**: 1154–1165

Stoppel R, Meurer J (2011) The cutting crew – ribonucleases are key players in the control of plastid gene expression. J Exp Bot **63**: 1663–1673

Stoppel R, Lezhneva L, Schwenkert S, Torabi S, Felder S, Meierhoff K, Westhoff P, Meurer J (2011) Recruitment of a ribosomal release factor for light- and stress-dependent regulation of petB transcript stability in Arabidopsis chloroplasts. Plant Cell **23**: 2680

Szabò I, Spetea C (2017) Impact of the ion transportome of chloroplasts on the optimization of photosynthesis. J Exp Bot **68**: 3115–3128

Sze H, Chanroj S (2018) Plant endomembrane dynamics: studies of K^{+}/H^{+} antiporters provide insights on the effects of pH and ion homeostasis. Plant Physiol **177**: 875–895.

Tadini L, Jeran N, Pesaresi P (2020) GUN1 and plastid RNA metabolism: learning from genetics. Cells **9**: 2307

Tiller N, Bock R (2014) The translational apparatus of plastids and its role in plant development. Mol Plant **7**: 1105–1120.

Tokumaru M, Adachi F, Toda M, Ito-Inaba Y, Yazu F, Hirosawa Y, Sakakibara Y, Suiko M, Kakizaki T, Inaba T (2017) Ubiquitin-proteasome dependent regulation of the GOLDEN2-LIKE 1 transcription factor in response to plastid signals. Plant Physiol **173**: 524

Trapnell C, Roberts A, Goff L, Pertea G, Kim D, Kelley DR, Pimentel H, Salzberg SL, Rinn JL, Pachter L (2012) Differential gene and transcript expression analysis of RNA-seq experiments with TopHat and Cufflinks. Nat Protocols **7**: 562–578

Trösch R, Barahimipour R, Gao Y, Badillo-Corona JA, Gotsmann VL, Zimmer D, Mühlhaus T, Zoschke R, Willmund F (2018)

Commonalities and differences of chloroplast translation in a green alga and land plants. Nat Plants **4**: 564–575

Tsujii M, Kera K, Hamamoto S, Kuromori T, Shikanai T, Uozumi N (2019) Evidence for potassium transport activity of Arabidopsis KEA1-KEA6. Sci Rep **9**: 10040

Waters MT, Moylan EC, Langdale JA (2008) GLK transcription factors regulate chloroplast development in a cell-autonomous manner. Plant J **56**: 432–444

Waters MT, Wang P, Korkaric M, Capper RG, Saunders NJ, Langdale JA (2009) GLK transcription factors coordinate expression of the photosynthetic apparatus in Arabidopsis. Plant Cell **21**: 1109

Woodson, JD (2016) Chloroplast quality control - balancing energy production and stress. New Phytol **212**: 36–41

Woodson JD, Chory J (2008) Coordination of gene expression between organellar and nuclear genomes. Nat Rev Genet **9**: 383–395

Yon Rhee S, Beavis W, Berardini TZ, Chen G, Dixon D, Doyle A, Garcia-Hernandez M, Huala E, Lander G, Montoya M, et al. (2003) The Arabidopsis Information Resource (TAIR): a model organism database providing a centralized, curated gateway to Arabidopsis biology, research materials and community. Nucleic Acids Res **31**: 224–228

Zhang J, Yuan H, Yang Y, Fish T, Lyi SM, Thannhauser TW, Zhang L, Li L (2016) Plastid ribosomal protein S5 is involved in photosynthesis, plant development, and cold stress tolerance in Arabidopsis. J Exp Bot **67**:2731–2744

Zhou W, Cheng Y, Yap A, Chateigner-Boutin A-L, Delannoy E, Hammani K, Small I, Huang J (2009) The Arabidopsis gene YS1 encoding a DYW protein is required for editing of rpoB transcripts and the rapid development of chloroplasts during early growth. Plant J **58**: 82–96

Zhu JK, Liu JP, Xiong LM (1998) Genetic analysis of salt tolerance in Arabidopsis: evidence for a critical role of potassium nutrition. Plant Cell **10**: 1181–1191

Zhu X, Pan T, Zhang X, Fan L, Quintero FJ, Zhao H, Su X, Li X, Villalta I, Mendoza I, et al. (2018) K(+) Efflux antiporters 4, 5, and 6 mediate pH and K^+ homeostasis in endomembrane compartments. Plant Physiol **178**: 1657–1678

Zoschke R, Bock R (2018) Chloroplast translation: structural and functional organization, operational control and regulation. Plant Cell **30**:745–770

Zoschke R, Watkins KP, Barkan A (2013) A rapid ribosome profiling method elucidates chloroplast ribosome behavior in vivo. Plant Cell **25**: 2265–2275